SUPPLEMENTAL INFORMATION

Dynamic action potential clamp predicts functional separation in mild familial and severe *de novo* forms of *SCN2A* epilepsy

PATIENTS

The study was approved by the Human Research Ethics Committee of Austin Health, Melbourne. Nineteen individuals with the R1882Q or R853Q *SCN2A* mutations were identified from the literature, and from an *SCN2A* support group (www.scn2a.org).

Clinical data was collated from the literature for previously reported individuals (N = 14), with updated clinical information obtained in one patient. Individuals whose clinical data was not previously published (N = 5), had their mutations identified through clinical testing. Detailed phone or clinical interviews with these parents were undertaken by paediatric epileptologists (KBH, MRC), home videos were reviewed and medical records from the treating neurologist obtained. Mutations were confirmed de novo in 15 patients, inheritance was unknown in four. The age at last review was known in 13 patients with a median age of 6.5 years (range 5 months – 25 years). One patient was deceased.

Individuals with **R1882Q** mutations had early-onset developmental and epileptic encephalopathies (DEE) with focal seizures beginning on the first day of life; some showed marked improvement with phenytoin, and some had benefit with other sodium channel blockers. However, despite improved seizure control with phenytoin, there was no difference in developmental impairment in responders compared with non-responders, suggesting that seizure control is not sufficient to reverse the developmental impairment associated with the SCN2A mutation. All but one had severe to profound developmental delay, consistent with the 'severe neonatal-infantile' phenotype previously reported, whereas the milder phenotype in one infant was that of the 'intermediate neonatal-infantile' group (1).

Seizure onset occurred on day one of life in all patients with an R1882Q mutation (Table S1). Focal seizures were the initial seizure type in five; initial seizure type was unknown in two. The epileptic syndrome at onset was early infantile epileptic encephalopathy (EIEE) in three, unclassified in three and unknown in one. Seizure types evolved in six patients, including to infantile spasms in two. Seizures were ongoing at last review in the five patients for whom this information was available. Phenytoin use was reported in five patients, with improved seizure control in two and no definite effect on seizures in three. It should be noted though, that information on the doses used and blood levels reached was not available to determine whether a 'therapeutic dose' had been reached. One patient with no improved seizures had 'continuous thrashing' with phenytoin loads, being presumably an exacerbation of the movement disorder. Seizures were improved with carbamazepine in one. Two patients did not report improvement with any sodium channel blocker. At last review, six patients had severe developmental delay, and one moderate. A movement disorder was present in three patients (opisthotonus and dystonia (1), opisthotonus and oculogyric crises (1), 'thrashing movements' (1)), absent in one, and unknown in three. Other common features included hypotonia (4, one of whom also had episodic appendicular hypertonia), acquired microcephaly (3) and constipation (2). Two patients had normal brain imaging, one a subtle cortical dysplasia and one had T2 hyperintensities in the white matter, T1 hyperintensity in the basal ganglia and elongated superior temporal sulci.

www.pnas.org/cgi/doi/10.1073/pnas.1800077115

Individuals with the **R853Q** mutation had later-onset DEE, with median onset of seizures at the age of 8 months, usually preceded by some degree of developmental delay. The seizure type at onset was epileptic spasms in most. In these individuals, the response to sodium channel blockers was mixed. Seizures did not improve with phenytoin; indeed, worsening was reported in one. Improved seizure control was, however, reported with other sodium channel blockers in three patients (lamotrigine, carbamazepine, both rendering a patient seizure-free; and oxcarbazepine). Movement disorders, such as dystonia, were seen in both groups; however, severe choreoathetosis only occurred with the R853Q mutation. In two of these patients, the choreoathetosis preceded seizure onset. In both groups, most patients had other types of seizures arising over time, refractory seizures and significant developmental delay.

Four previously published patients with R853Q mutation had minimal available clinical information. Two were listed as having an epileptic encephalopathy, one West syndrome (WS) and one Lennox Gastaut syndrome (LGS). More detailed clinical data was available on eight patients (Table S2). For these individuals, seizure onset occurred at a median age of eight months (range 6 months – 3 years). The initial seizure type was infantile spasms in six, infantile spasms and tonic seizures in one, and tonic seizures in one. The epileptic syndrome at seizure onset was WS in seven and unclassified in one. Evolution to other seizure types was reported in seven patients, each having multiple seizure types. After evolution of seizures, the epilepsy syndrome was unclassified or unknown in all but one patient, who had LGS. Phenytoin use was reported in three patients, with no effect in two and exacerbation of seizures in one. Six patients had used other sodium channel blockers. Seizure exacerbation was noted in only one patient (on carbamazepine). One was seizure free on lamotrigine and seizure control improved on carbamazepine in one. One patient had improvement of seizures on low dose oxcarbazepine; at higher dose, seizure control remained good but there was marked worsening of overall motor function and of stimulatory behaviours. ACTH was beneficial in four patients; vigabatrin was beneficial in one and exacerbated seizures in three. Seven individuals had ongoing seizures at last review, although reduction in seizure frequency from age four years was noted in three. Development was delayed prior to seizure onset in six patients, normal in one and unknown in one. At last review, all patients had severe developmental delay. All individuals had a movement disorder; four had choreoathetosis two dystonia and two a mixed movement disorder. For three patients in whom further information on the movement disorder was available, the movement disorder had onset in infancy, predating seizure onset in two, and remaining a major medical issue in all three. Improvement was noted with L-Dopa/Carbidoba and cannabis (high CBD, low THC preparation) in one and triheptanoin in another. Additional features included hypotonia (5), severe vomiting and failure to thrive in infancy (3), microcephaly (2), extreme irritability (2) and episodic agitation with red, hot areas of the body (2). Brain imaging was normal in three, showed atrophy in three, thin or hypoplastic corpus callosum in two, areas of hyperintensity on T2-weighted imaging in two and white matter volume loss in one.

Table S1. Clinical features and treatment response in the newly identified and previously published patients with R1882Q mutation (N = 7)

Reference and patient (p)	Mutation inheritance	Age at last review	Age epilepsy onset (+/- severity)	Onset seizure type	Onset epileptic syndrome	Later seizure type	Later epileptic syndrome	PHT response	Other sodium channel blocker response	Other AED response	Ongoing seizures at last review?	Movement disorder/ paroxysmal neurological symptoms	Development pre-seizure onset	Development at last review (+/- autism)	MRI	Other
(1, 4) This study (p1)	*de novo*	21 months (deceased)	1 day	F	EIEE	T	Unclassified	Benefit	None beneficial	None beneficial	Yes	Opisthotonus, oculogyric crises	N/A (too young)	Delayed (severe)	T2 hyperintensity in white matter, T1 hyperintensity in basal ganglia, elongated superior temporal sulci	Axial hypotonia, intermittent appendicular hypertonia, acquired microcephaly, extreme irritability, severe constipation
(1) This study (p2)	*de novo*	3 years	1 day	F	Unclassified	F	Unclassified	Benefit	None beneficial	Benefit with triheptanoin, CBD	Yes	Nil	N/A (too young)	Delayed (moderate)	Normal	Hypotonia, sensory issues
This study (p3)	*de novo*	5 years	1 day	F	Unclassified	F, autonomic, gelastic	Unclassified	No definite benefit, movement disorder ('continuous thrashing') with phenytoin loads	None beneficial	Benefit with VPA	Yes	'Thrashing' movements	N/A (too young)	Delayed (severe)	n.a.	Hypotonia, constipation, respiratory issues
This study (p4)	UK	5 months	5 months	F	Unclassified	F, T, Sp	Unclassified	No definite benefit	None beneficial	None beneficial	Yes	Opisthotonus, dystonia	N/A (too young)	Delayed (severe)	Normal	Hypotonia, excess startle, elevated liver transaminases
(7) (p1)	*de novo*	n.a.	1 day	F	EIEE	Sp, T, TCS, gelastic	n.a.	n.a.	n.a.	n.a.	n.a.	n.a.	N/A (too young)	Delayed (severe)	n.a.	Microcephaly
(7) (p2)	*de novo*	n.a.	1 day	'neonatal seizures'	EIEE	T, apnoeic	n.a.	n.a.	n.a.	n.a.	n.a.	n.a.	N/A (too young)	Delayed (severe)	n.a.	n.a.
(6)	UK	10.5 years	1 day	Not applicable	n.a.	F, C	n.a.	No effect	CBZ - seizure reduction, OXC and LTG - no effect	None beneficial	Yes	n.a.	N/A (too young)	Delayed (severe)	Subtle cortical dysplasia	Microcephaly

Abbreviations. AED, anti-epileptic drug; C, clonic; CBZ, carbamazepine; EIEE, Early infantile epileptic encephalopathy; F, focal; LTG, lamotrigine; MRI, magnetic resonance imaging; n.a., not available,; N/A, not assessed; OXC, oxcarbazepine; PHT, phenytoin; Sp, spasms; T, tonic; TCS, tonic clonic seizures; VPA, valproic acid

Table S2. Clinical features and treatment response in the newly identified and previously published patients with R853Q mutation (N = 12)

Reference and patient (p)	Mutation inheritance	Age at last review	Age epilepsy onset (+/- severity)	Onset seizure type	Onset epileptic syndrome	Later seizure type	Later epileptic syndrome	PHT response	Other sodium channel blocker response	Other AED response	Ongoing seizures at last review?	Movement disorder/ paroxysmal neurological symptoms	Development pre-seizure onset	Development at last review (+/- autism)	MRI	Other
This study (p1)	*de novo*	6 years	6 months	Sp	WS	T, Sp	Unclassified	Not used	CBZ - benefit	None beneficial, VGB exacerbated seizures	Yes (but rare after 4 years old, EEG remains abnormal)	Choreoathetosis (onset 9 months, benefit with L-Dopa/Carbidopa and cannabis (high CBD, low THC preparation))	Delayed (mild)	Delayed (severe)	White matter volume loss, thin corpus callosum	Hypotonia, vomiting and FTT
This study (p2)	*de novo*	7 years	8 months	Sp, T	WS	T, Sp, M	Unclassified	Exacerbated seizures	OXC - benefit at low dose, at high dose seizures still controlled but marked worsening of motor function and stimulatory behaviours	Benefit with ACTH, THC, triheptanoin. VGB exacerbated seizures.	Yes (but infrequent after 4 years old, EEG normal)	Choreoathetosis (onset early infancy, more obvious since seizures have settled, benefit with triheptanoin)	Delayed (mild)	Delayed (severe)	Normal	Vomiting (ceased transiently with ACTH, then permanently at 3 years old) and FTT, hypotonia, extreme irritability, episodes of agitation with red, hot ears lasting minutes to hours, hypersensitivity to touch, strabismus (resolved), mildly abnormal liver function tests
This study (p3)	UK (parents not tested)	12 years	6 months	Sp	WS	T, F, M	Unclassified	No effect	n.a.	Benefit with paraldehyde (for treatment of long clusters of seizures), VGB exacerbated seizures, ACTH no effect	Yes (but less frequent after 4 years old)	Choreoathetosis (onset early infancy)	Delayed	Delayed (severe)	Normal	Vomiting and FTT, hypotonia, extreme irritability (some improvement with VPA, GBP and amitriptyine), episodic agitation with migrating red, hot areas of body, hypersensitivity to touch and noise
(6) (p1)	*de novo*	6.5 years	8 months	Sp	WS	AA, T, F	LGS	Not used	CBZ - exacerbated seizures	Benefit with ACTH (seizure free - presumably means spasm free), VPA, CLB, TPM	Yes	Dystonia	Normal	Delayed (severe)	Atrophy, T2 hyperintensities (? Regions)	Microcephaly, preterm infant
(6) (p2)	*de novo*	8 years	13 months	Sp	WS	T, autonomic, M	UK (EEG called 'CSWS-like')	No effect	OXC, LTG - no effect	Benefit with VGB, CLB, PB	Yes	Choreoathetosis	Delayed (moderate)	Delayed (severe)	Normal	Hypotonia
(6) (p3)	UK	25 years	3 years	T	Unclassified	Sp	n.a.	n.a.	n.a.	Benefit with ACTH, VPA	Yes	Hand dystonia	Delayed (severe)	Delayed (severe)	CC hypoplasia	Pyramidal signs, arachnodactyly
(3) (p1)	*de novo*	n.a.	n.a.	n.a.	LGS	n.a.	n.a.	n.a.	n.a.	n.a.	n.a.	n.a.	n.a.	n.a.	n.a.	n.a.
(3) (p2)	*de novo*	n.a.	n.a.	Sp	WS	n.a.	n.a.	n.a.	n.a.	n.a.	n.a.	n.a.	n.a.	n.a.	n.a.	n.a.
(2, 8)	*de novo*	UK (> 6 years)	10 months	Sp	WS	n.a.	n.a.	n.a.	LTG – seizure free	n.a.	No (seizure free from 6 y 2 m, after LTG)	Dystonia, chorea, ballismus	n.a.	Delayed (severe)	Cerebral and cerebellar atrophy, thin corpus callosum	n.a.
(5)	*de novo*	2 years	8 months	Sp	WS	F, M	n.a.	n.a.	LTG - 'remained intractable'	Benefit with ACTH (ceased spasms)	Yes	Dystonia, chorea	Delayed	Delayed (severe)	Atrophy, T2 hyperintensities BG and thalamus	Hypotonia, microcephaly
(9) (p1)	*de novo*	n.a.	n.a.	n.a.	n.a.	n.a.	n.a.	n.a.	n.a.	n.a.	n.a.	n.a.	n.a.	n.a.	n.a.	Listed as 'EE' with no further information provided
(9) (p2)	*de novo*	n.a.	n.a.	n.a.	n.a.	n.a.	n.a.	n.a.	n.a.	n.a.	n.a.	n.a.	n.a.	n.a.	n.a.	Listed as 'EE' with no further information provided

Abbreviations (**Tables 1 and 2).** AA, atypical absence; AED, anti-epileptic drug; ACTH, adrenocorticotropic hormone; CC, corpus callosum; CBD, cannabidiol; CBZ, carbamazepine; CLB, clobazam; CSWS, continuous spike wave in sleep; EEG, electroencephalogram; EE, epileptic encephalopathy; F, focal; FTT, failure to thrive; GBP, gabapentin; LTG, lamotrigine; LGS, Lennox-Gastaut syndrome, M, myoclonic; MRI, magnetic resonance imaging; n.a., not available; OXC, oxcarbazepine; PB, phenobarbital; PHT, phenytoin; Sp, spasms; T, tonic; THC, tetrahydrocannabinol; TPM, topiramate; UK, unknown; VGB, vigabatrin; VPA, valproic acid; WS, West syndrome

PLASMIDS

The SCN2A plasmid encoding the adult isoform of the human Nav1.2 channel (pcDNA3.1(+)-Nav1.2) has been previously described (10). The R853Q mutation is located in the voltage sensor of domain 2. L1563V is in the second segment of domain 4, and R1882Q in the COOH terminus (Fig. 1A). The R853Q mutation was introduced with QuikChange site-directed mutagenesis (Agilent Technologies, Santa Clara, CA) using forward and reverse primers GTTCTCCGATCATTCCAGCTGCTCCGAGTTTTC and GAAAACTCGGAGCAGCTGGAATGATCGGAGAAC, respectively. The pcDNA3.1(+) plasmids, containing the human Nav1.2 channel with the L1563V or R1882Q mutations, were generated commercially (TOP Gene Technologies, Quebec, Canada). All clones were verified by automated DNA sequencing (Australian Genome Research Facility).

CELL CULTURE AND TRANSFECTIONS

Chinese hamster ovary (CHO) cells were cultured in Dulbecco's Modified Eagle Medium: Nutrient Mixture F-12 (Thermo Fisher Scientific, Waltham, MA) supplemented with 10% (v/v) fetal bovine serum (Thermo Fisher Scientific) and 50 IU/ml penicillin (Thermo Fisher Scientific) at 37°C with 5% CO_2. The cells were grown in T25 cm^2 flasks (BD Biosciences, San Jose, CA, USA) to ~80 % confluency, and then transiently co-transfected with wild-type or mutant pcDNA3.1(+)-$Na_v1.2$ (4 μg) and enhanced green fluorescent protein (eGFP; 1 μg; Clontech, Mountain View, CA), using Lipofectamine 3000 Reagent (Thermo Fisher Scientific). After transfections, cells were incubated at 37°C in 5% CO_2. 24 hours post-transfection, the cells were detached using TrypLE Express Reagent (Thermo Fisher Scientific), plated on 13 mm diameter glass coverslips (Menzel-Gläser, Thermo Fisher Scientific), and incubated at 30°C in 5% CO_2. Electrophysiological recordings were performed 48 to 72 hours post transfection.

ELECTROPHYSIOLOGY

Cells were placed into a ~0.1 ml recording chamber and superfused with extracellular solution at a constant rate of ~0.2 ml/min. The extracellular bath solution contained 145 mM NaCl, 5 mM CsCl, 2 mM $CaCl_2$, 1 mM $MgCl_2$, 5 mM glucose, 5 mM sucrose, 10 mM Hepes (pH = 7.4 with NaOH and osmolarity of ~305 mosmol l^{-1}), whereas the intracellular solution contained 5 mM CsCl, 120 mM CsF, 10 mM NaCl, 11 mM EGTA, 1 mM $CaCl_2$, 1 mM $MgCl_2$, 2 mM Na_2ATP, 10 mM Hepes (pH = 7.3 with CsOH and osmolarity of ~290 mosmol l^{-1}).

Experiments were performed at room temperature (23 ± 0.5 °C) set by a TC344B Dual Automatic Temperature Controller (Warner Instruments, Hamden, CT). Patch electrodes were pulled from borosilicate glass capillaries (GC150TF-7.5, Harvard Apparatus Ltd.) and typically exhibited resistance values of 1.2–1.5 MΩ. Liquid junction potentials were corrected and series resistance values, typically of 2–2.5MΩ, were 90–95% compensated. To minimize possible voltage errors, only relatively small CHO cells of 15–25 pF cell capacitance (C_m = 22 ± 1 pF, n = 168), expressing peak I_{Na} amplitudes larger than 2 nA but smaller than 10 nA, were selected. I_{Na} amplitudes that fall outside the selected range would introduce errors in dynamic action potential clamp experiments (see below). Approximately 10-20 % of the transfected cells showing green fluorescence did not express functional ion channel protein or exhibited peak I_{Na} values of very small (a few tens to a hundred pA) to small (<2 nA) amplitudes, and were excluded from analysis. Cells with peak I_{Na} values exceeding 10 nA, recorded in ~5-10 % of cells expressing wild-type or L1563V channels, in less than 5% in cells expressing R853Q channels, and in ~10-20% of cells expressing R1882Q channels, were also excluded. Finally, cells were excluded from the analysis if the amplitude of the leak current at a holding potential (HP) of −120 mV was larger than 2% of the peak I_{Na}. The contribution of endogenous I_{Na} to the total I_{Na} was considered as negligible (11). The leak and capacitive currents were corrected using a −P/4 pulse protocol unless mentioned otherwise. In the experiments using tetrodotoxin, I_{Na} was determined as the current blocked by 100 nm tetrodotoxin (Alomone Laboratories, Israel).

The current density, voltage dependence of I_{Na} activation and inactivation, recovery from inactivation, and development of slow inactivation were determined using the voltage protocols depicted in the figures and explained in the Results. In most voltage clamp experiments, the HP was −120 mV; however recovery from inactivation was determined from HP values of −120 and −70 mV, because recovery is voltage dependent (12) and, in dynamic clamp experiments (see below), the free running resting membrane potential (V_m) of the AIS compartment model cell was approximately −70 mV. Peak I_{Na} was defined as the difference between peak and steady-state currents recorded during depolarization and when keeping the cell at HP, respectively. Current-voltage (I–V) relationships were determined by measuring peak I_{Na} during 40-ms depolarizing voltage steps ranging from –80 to +60 mV, at 0.5 Hz. Peak I_{Na} was converted to peak conductance by the equation $G = I/(V\text{-}V_{rev})$, where V_{rev} is the sodium channel reversal potential. The resulting normalized conductance-voltage relationships are plotted as G/G_{max} values versus voltage and are referred to as 'activation' curves. The voltage dependence of steady-state fast inactivation was obtained using pre-pulses of 100 ms duration in 5 mV increments in the voltage range between −120 and +10 mV, followed by a 10-ms voltage step to −5 mV. Steady-state activation and inactivation curves were fit using the Boltzmann equation:

$$\frac{G}{G_{max}} = \frac{1}{[1+e^{(V-V_{0.5})/k}]},$$

where V is the conditioning voltage, $V_{0.5}$ is the half-maximal (in)activation voltage, and k is a slope factor. The steady-state open probability (P_o) was estimated in the voltage range between −100 mV and +40 mV in 5 mV increments, by multiplying the values of fractional activation and inactivation. Results were expressed as the m × h product as a function of V_m (13) and were fit with a bi-Gaussian peak function:

$$m = A\, e^{-0.5[\frac{x-x_c}{w_1}]^2}, x < x_c, \text{ and}$$

$$h = A\, e^{-0.5[\frac{x-x_c}{w_2}]^2}, x \geq x_c,$$

where m represents the probability that the channel is activated, and h is the probability that a channel is not inactivated, A represents the peak (height) of the curve, x_c represents the V_m value corresponding to the peak of the fitted curve, w_1 and w_2 represent the width of the V_m range of m and h, respectively. It should be noted that the m parameter for activation is derived directly from the measurement of G/G_{max}, different from the Hodgkin-Huxley m parameter based on m^3 kinetics. The magnitude of the window current was estimated by calculating the overlapping area under the Boltzmann equations describing the activation and inactivation, in the voltage range between −100 mV and +60 mV as follows:

$$\text{Area} = \int_{-100}^{V_0} \frac{1}{1+e^{((V-V_{0.5,act})/k_{act})}}\, dV + \int_{V_0}^{+60} \frac{1}{1+e^{((V-V_{0.5,inact})/k_{inact})}}\, dV,$$

where V_0 is the voltage value where the crossover of the activation and inactivation curves occurs, k_{act} and k_{inact} are the slope factors of activation and inactivation, respectively, $V_{0.5,act}$ and $V_{0.5,act}$ are the V_m values for half-maximal voltage of activation and inactivation, respectively. The window current was expressed as percent of total area (Table 2). It should be noted that this procedure is only an approximate method to predict steady-state current, because the activation curve does not accurately represent steady-state activation, as it is derived from a measurement of non-steady-state peak transient current, where activation may not be at steady-state and inactivation has already progressed to some degree. Persistent I_{Na}, expressed as percent of peak I_{Na}, was determined at 40 ms after the onset of the step voltage command by either subtracting traces recorded in the presence of tetrodotoxin from control, or by estimating inward I_{Na} after –P/4 leak correction. Both methods resulted in similar values and for comprehensive mutant and wild-type data analysis the –P/4 method was used. To determine the time constants of peak I_{Na} inactivation elicited at various voltages, the time course of individual I_{Na} traces was fitted with a double-exponential equation:

$$\frac{I}{I_{max}} = A_f e^{-t/\tau_f} + A_s e^{-t/\tau_s},$$

where t is time, A_f and A_s are the fractions of the fast and slow inactivation components, and τ_f and τ_s are the time constants of the fast and slow inactivating components, respectively. The fast time constant (τ_f) was plotted against the test potential V, in the range between −40 mV and +10 mV. Voltage dependence of recovery from (fast) inactivation was assessed from HP values of either −120 or −70 mV with a paired-pulse protocol comprising a 10 ms pre-pulse to −10 mV (P1), which served to fast-inactivate the I_{Na}, followed by a test pulse to −10 mV (P2), to measure I_{Na} availability after variable recovery intervals. Recovery was analysed by fitting a single exponential function to the data to obtain the time constant, τ as follows:

$$\frac{I}{I_{max}} = 1 - e^{-t/\tau},$$

where t is time (here the delay between pre-pulse P1 and test pulse P2). To evaluate the rate of entry into slow inactivation that develops during prolonged membrane depolarization or repeated high-frequency firing (14, 15), the HP was kept at −60 mV for time intervals of increasing duration (0.005s-195s). Between the intervals, the membrane was hyperpolarized to −120 mV for 20 ms, allowing channels recover from fast inactivation, and then I_{Na} availability was assessed with a 2-ms test pulse to −10 mV. In similar experiments, we also determined the entry into slow inactivation at −50 mV for wild-type and mutant currents, respectively. The development of slow inactivation was evaluated by fitting data with the double-exponential equation above.

PARAMETERS OF ACTION POTENTIALS AND INPUT I_{Na} IN DYNAMIC CLAMP EXPERIMENTS

Rheobase was determined as the minimal stimulus current needed to elicit an action potential. Input-output relationships were determined as the number of action potentials elicited during injections of step currents of 500 ms or 1 s duration, or as the firing frequency of the model cell in response to synaptic currents of various ge:gi ratios during 5 s recordings. Action potential upstroke velocity was defined as the maximum value of the first derivative of the action potential waveform. Action potential threshold was determined at the 10 mV/ms upstroke velocity value, using the first derivative method. The action potential half-width was measured as the period between the trace's crossing the half-amplitude point in its rising and decaying stages. The amplitude of the input I_{Na} was determined during action potential firing. All action potential and I_{Na} parameters were determined using Clampfit except action potential rise (upstroke velocity), which was estimated in Axograph X (Axograph Scientific, Sydney, Australia).

PORE CURRENT RECORDINGS

The extracellular bath solution contained 125 mM NaCl, 20 mM guanidine-sulfate, 2 mM $CaCl_2$, 1 mM $MgCl_2$, 10 mM Hepes (pH = 7.3 with NaOH), whereas the intracellular solution contained 135 mM CsF, 5 mM NaCl, 1 mM EGTA, 10 mM Hepes (pH = 7.3 with NaOH). In some experiments, the extracellular solution contained 60 mM guanidine-sulfate instead of 20 mM.

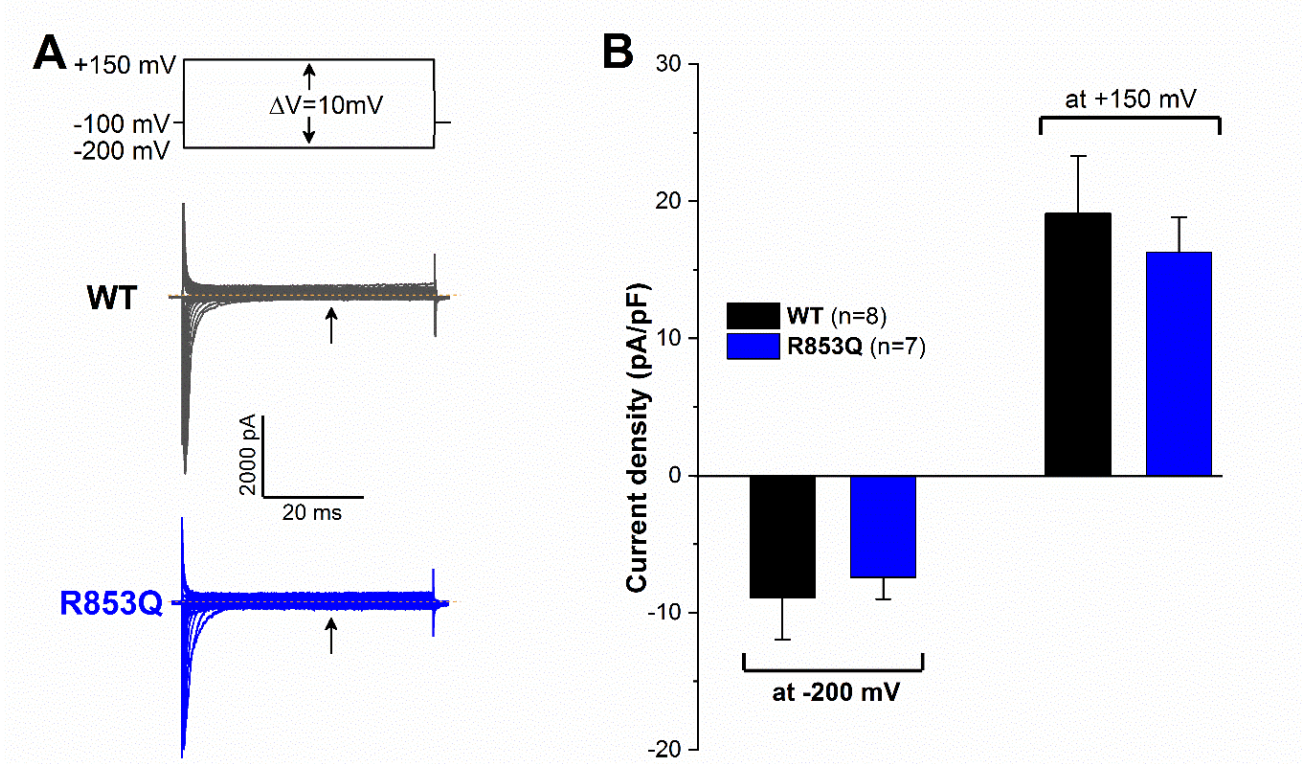

Supplemental Figure S1. Inward and outward currents in CHO cells transiently expressing wild-type or R853Q Nav1.2 channels. (**A)** Representative wild-type (WT) and R853Q I_{Na} traces, elicited by 50-ms voltage steps of 10 mV increment from a holding potential (HP) of –100 mV (top inset). To establish presence of pore currents, current amplitude was measured at 30 ms after the onset of the step voltage command (arrow). Dotted lines indicate zero current level; P/N leak subtraction was turned off. (**B)** Current densities determined at HP values of -200 and +150 mV, respectively. Increasing the concentration of guanidine-sulfate to 60 mM in the extracellular solution (16) did not affect the current amplitude (n = 3). Data are mean ± SEM; n, number of experiments between parentheses.

ROBUSTNESS OF THE AXON INITIAL SEGMENT (AIS) COMPARTMENT MODEL IN DYNAMIC ACTION POTENTIAL CLAMP EXPERIMENTS

To evaluate the effects of altering various model features on the firing activity in the presence of external wild-type or mutant $Na_v1.2$ channel current ($I_{Nav1.2}$) inputs, the capacitance (Cm) and/or the scaled individual conductances of the model cell were systematically varied. Cm was altered across a range from 0.5 to 1.5 of original parameter value, potassium channel's conductance (gKv) was altered from 0.25 to 7-fold from original, and $Na_v1.6$ channel conductance ($gNa_v1.6$) was changed from 0.2 to 1.5. We also altered the scaling of the input wild-type or mutant $I_{Nav1.2}$ from 0.6 to 1.2 to test the relationship between this parameter and the predictions of the model. The virtual $Na_v1.6$ current ($I_{Nav1.6}$) was set to zero unless stated otherwise and the model was run at 23°C to match $I_{Nav1.2}$ recording conditions. The external $I_{Nav1.2}$ and the virtual V_m, I_{syn}, g_e, g_i, I_{Kv}, and $I_{Nav1.6}$ were simultaneously recorded. Action potential firing was elicited in response to synaptic currents or in response to step current stimuli.

As expected, the firing frequency tracked with parameter value changes in a predictable fashion and no unexpected findings or strange bifurcations were observed, suggesting that the model itself was stable across this range of parameter values.

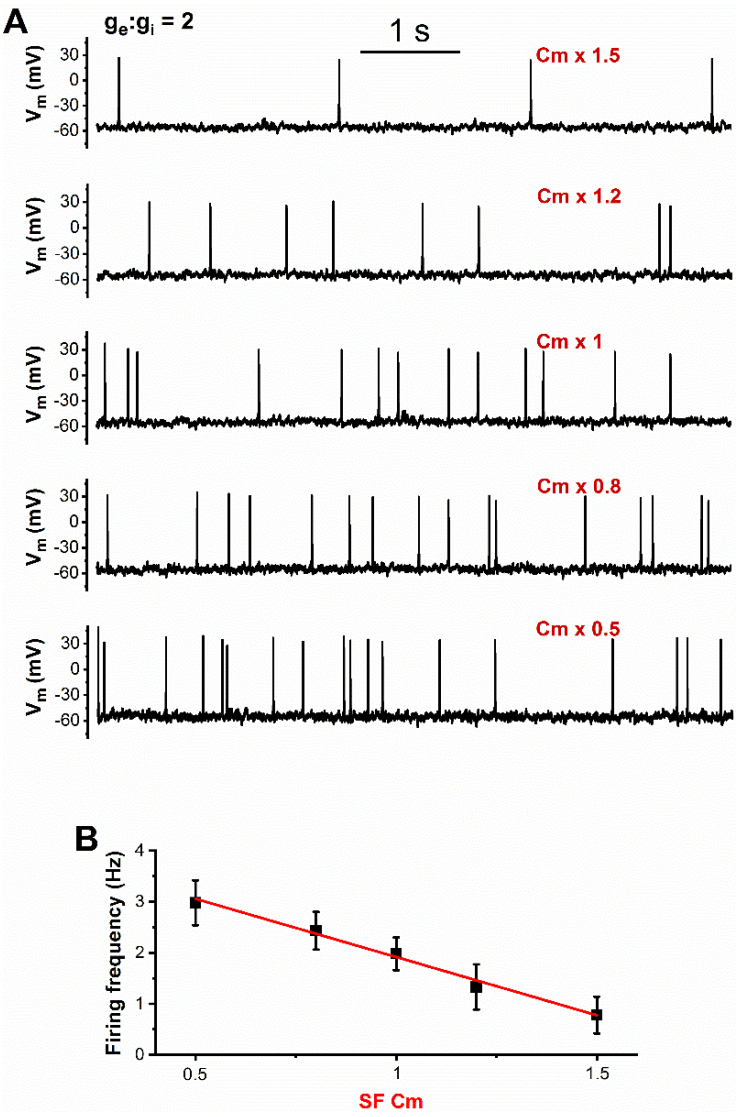

Supplemental Figure S2. Effects of varying the capacitance (Cm) of the AIS compartment on firing activity. **(A)** Reducing the Cm increases the firing rate. Representative firing responses elicited by a synaptic current of excitatory (g_e) to inhibitory (g_i) conductance ratio (g_e:g_i) of 2. The amplitude of the wild-type input $I_{Nav1.2}$ was set to 350-375 pA. **(B)** Relationship between the firing frequency and scaled Cm. Data are presented as mean ± SEM, n, number of independent experiments = 4. Data were fit with a linear equation of type y = mx + b, where m (slope) = –2.28 ± 0.14.

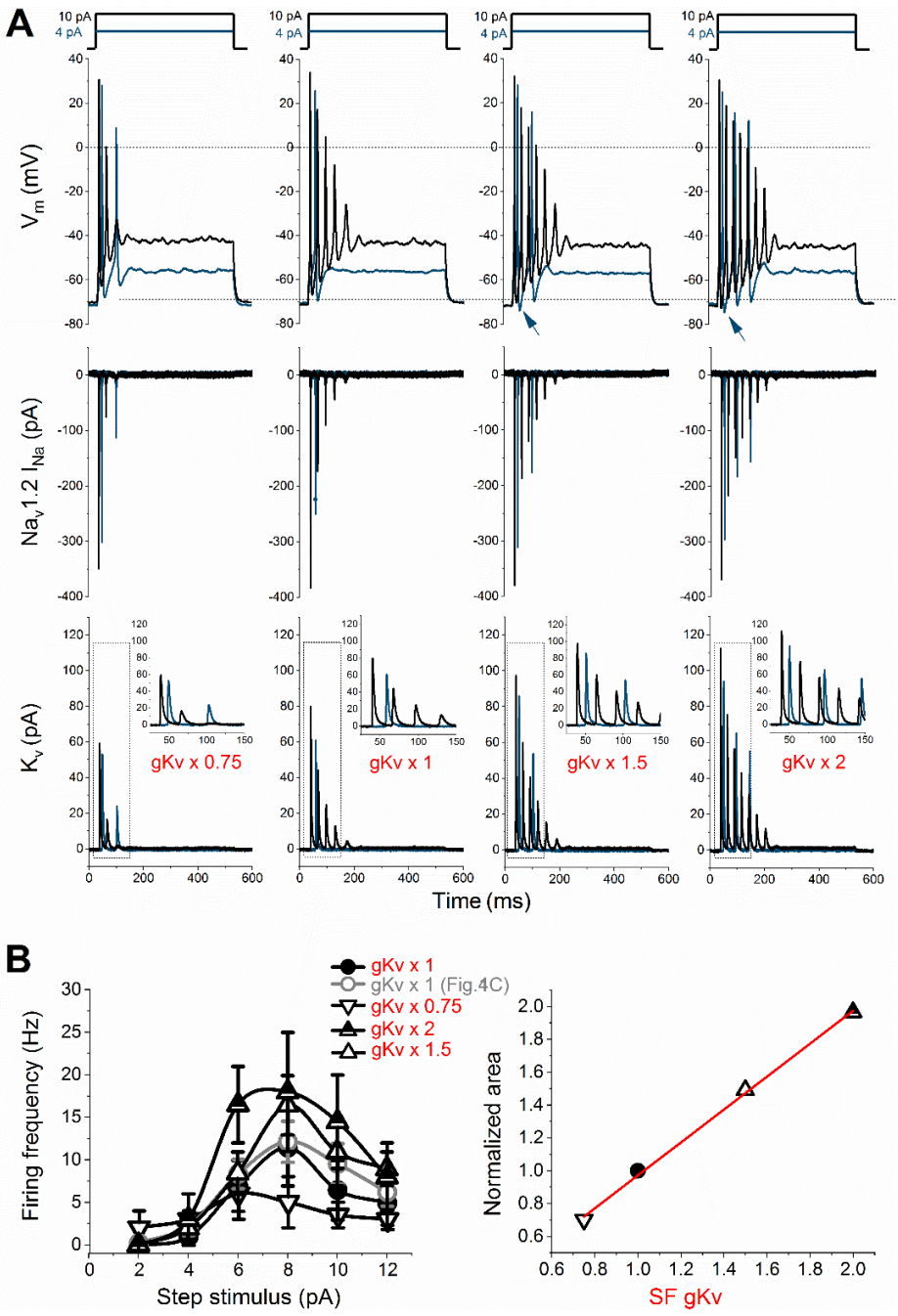

Supplemental Figure S3. The effect of altered gKv on AIS compartment model activity in response to step current (I_{st}) stimulation **(A)** Representative action potential firing (upward deflections, top), elicited by 4 or 10 pA I_{st} steps (top insets); associated wild-type input $I_{Nav1.2}$ (downward deflections, middle), and virtual potassium current (I_{Kv}) (upward deflections, bottom); note boxed I_{Kv} traces on an expanded time scale. **(B)** Input-output relationships with the original AIS model cell gKv scaled to the indicated values (left). Action potentials were elicited by I_{st} of 500 ms duration in 2 pA increments between 2 and 12 pA. Note that the input-output curve with wild-type input $I_{Nav1.2}$ from Fig. 4C is re-plotted for comparison (grey symbols). Data are presented as mean ± SEM; for each data point $n \geq 4$. Note the increase of firing activity with increasing gKv values. Relative to gKv < 1, the V_m is more efficiently repolarized below action potential threshold with gKv > 1 (arrows), facilitating the recovery of Na_v channels from inactivation. This transient repolarizing effect is counteracted by the I_{st} that efficiently depolarizes the V_m to threshold for action potential firing. Right: Relationship between overall firing and scaled gKv, expressed as the normalized area under the corresponding input-output curve shown in the left panel (slope of the linear fit is 1.00 ± 0.02).

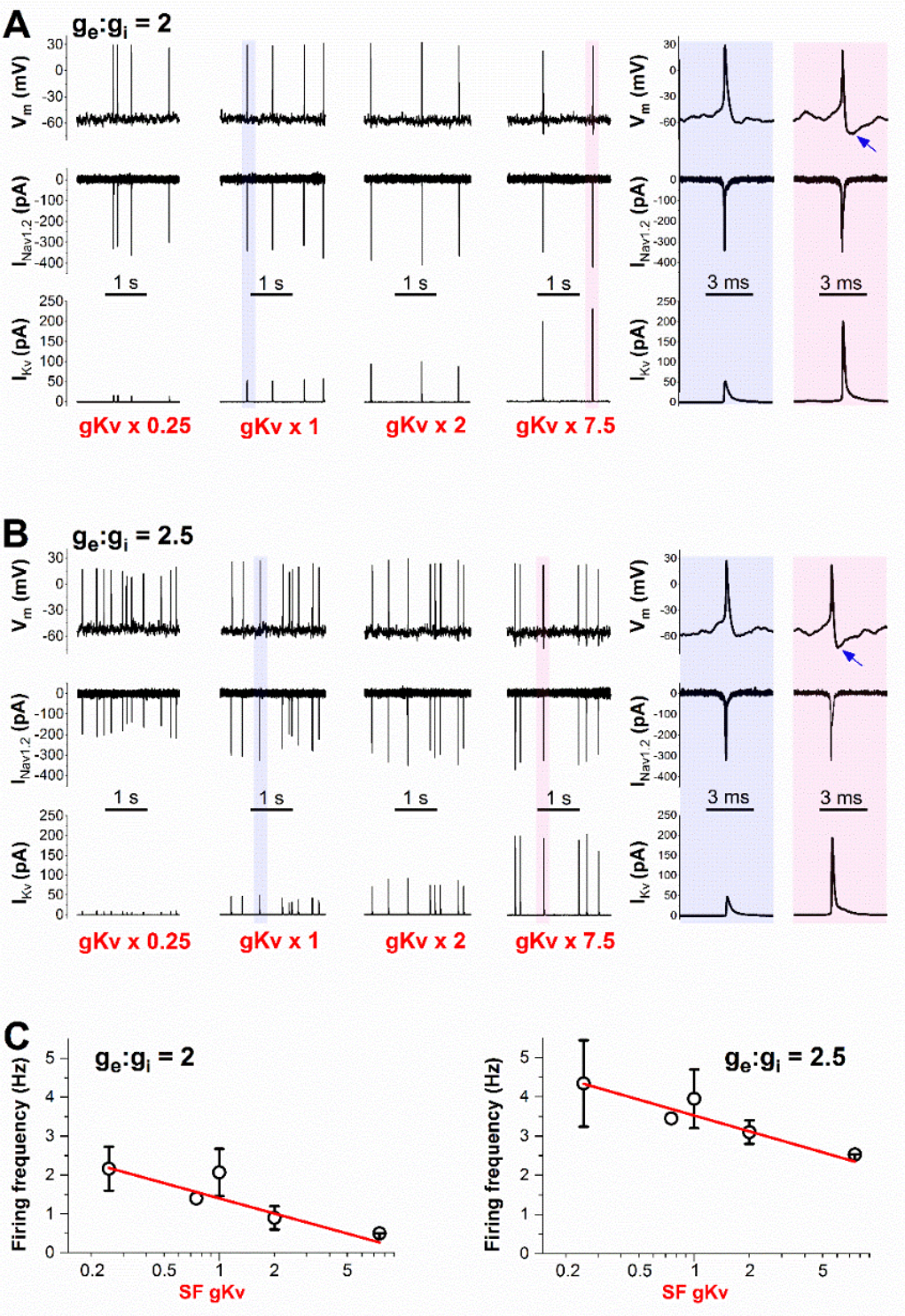

Supplemental Figure S4. The effect of scaling gKv on AIS compartment model activity in response to synaptic current stimulation. Representative examples of firing elicited with g_e:g_i = 2 **(A)** or g_e:g_i = 2.5 **(B)**, respectively. Right: shaded boxes show V_m, wild-type $I_{Nav1.2}$, and I_{Kv} traces on expanded time scale. **(C)** Input-output relationships as a function of g_e:g_i. Note that gKv scaling produces relatively small changes in firing frequency; large gKv values transiently hyperpolarize the membrane potential (arrows). Data are presented as mean ± SEM; for each data point n ≥ 4, except for SF = 0.8 and 7 (n = 1 for both). The slopes of the linear fits to the data were −1.29 ± 0.05 (left) and −1.34 ± 0.01 (right).

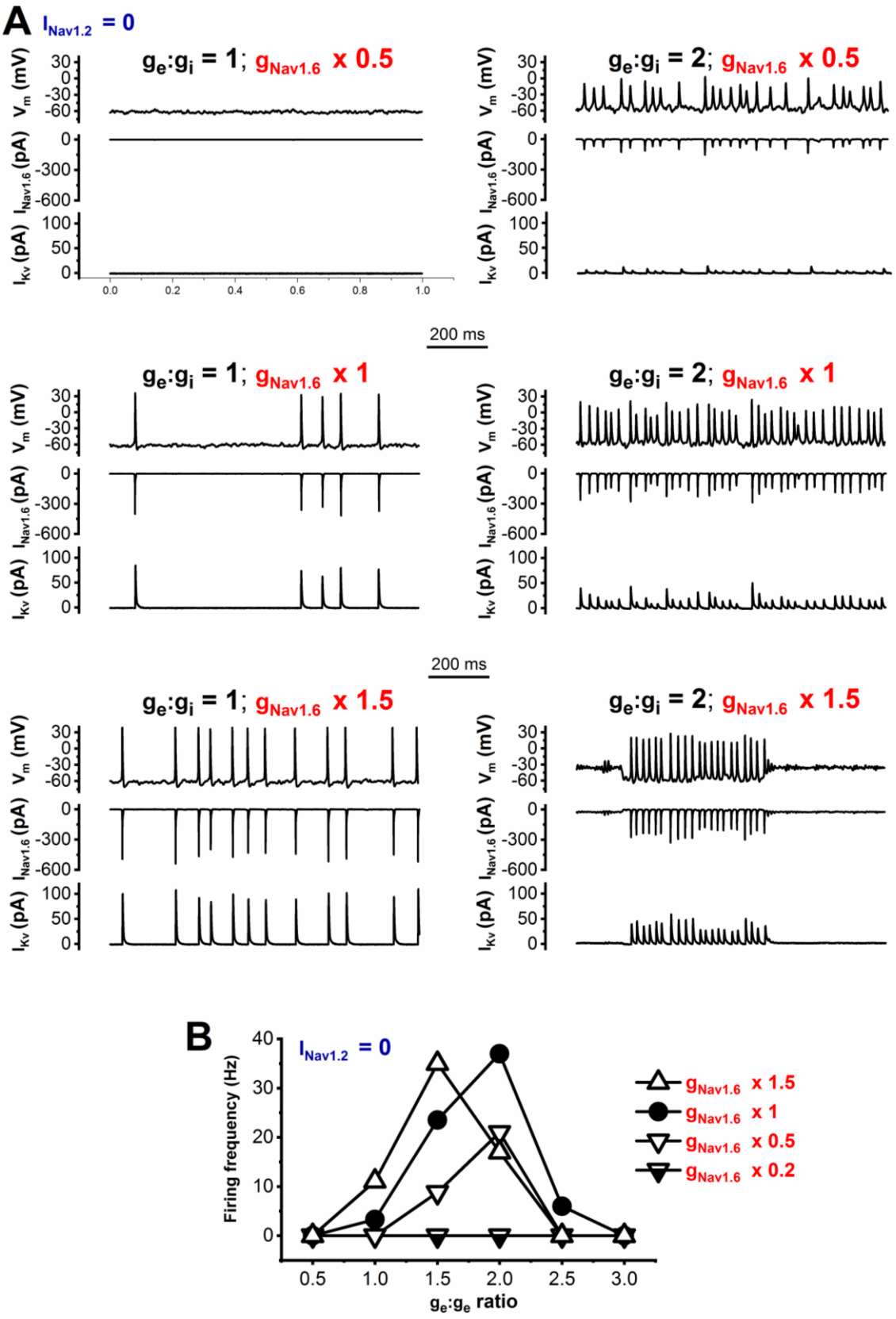

Supplemental Figure S5. The effect of scaling the virtual $I_{Nav1.6}$ on the AIS compartment model activity in response to synaptic stimulation. The external input $I_{Nav1.2}$ (also called I_{cell}; see Appendix) was set to zero. **(A)** Representative examples of V_m changes, associated $I_{Nav1.6}$ and I_{Kv} traces, elicited at g_e:g_i = 1 or 2, respectively. The effects of reducing control ($g_{Nav1.6}$ = 1) by 50 % or increasing it by 50 %, respectively, are shown. **(B)** Input-output relationships as a function of g_e:g_i ratios, with $I_{Nav1.6}$ scaled to the indicated values. Data represent mean; for each data point n = 2.

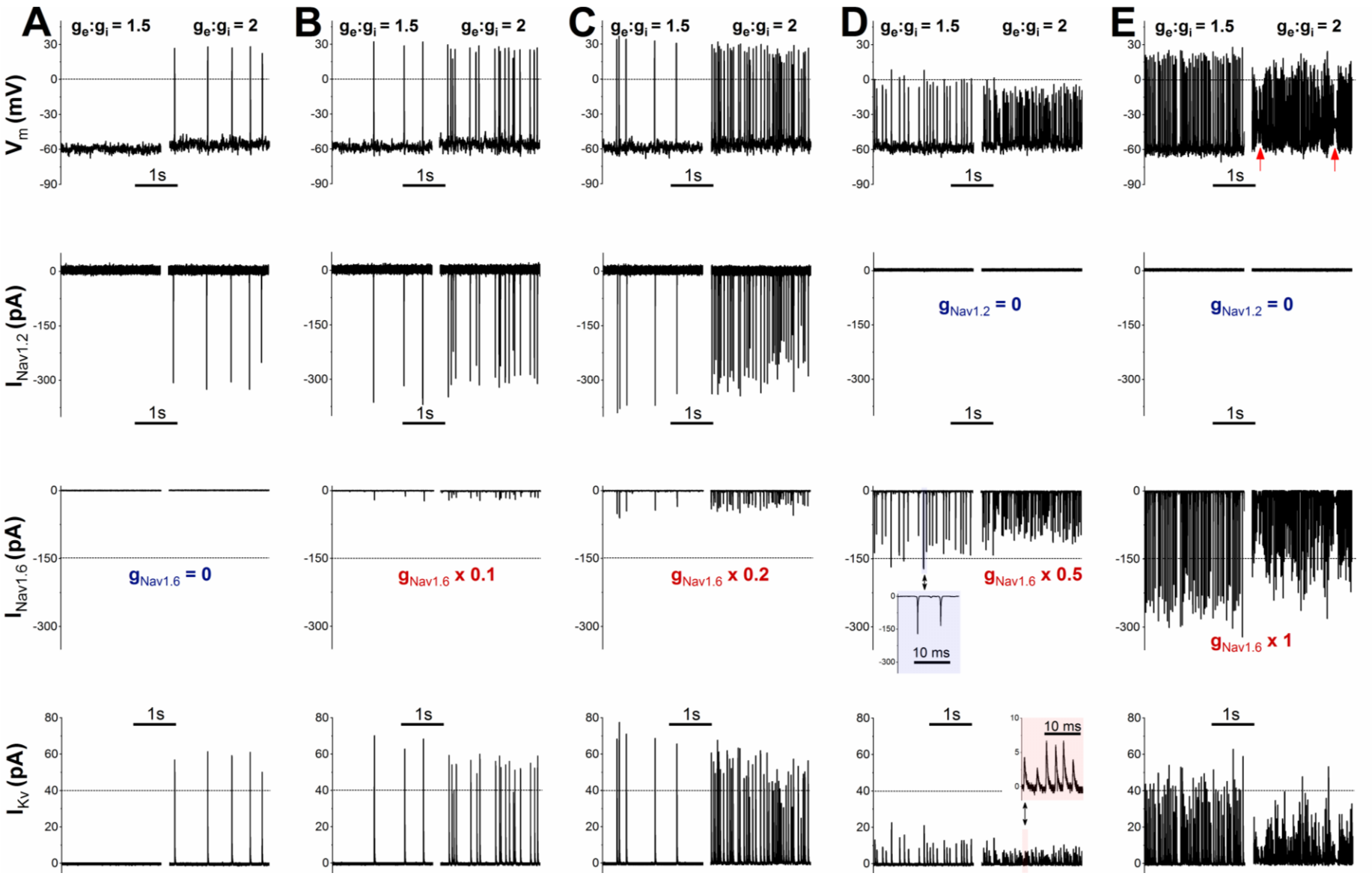

Supplemental Figure S6. The contribution of heterologously expressed wild-type $I_{Nav1.2}$ and/or virtual $I_{Nav1.6}$ to AIS compartment model activity. Activity is sensitive to the magnitude of individual $Na_v1.2$ and $Na_v1.6$ conductances. Representative V_m changes (upward deflections, first row), associated wild-type input $I_{Nav1.2}$ (downward deflections, second row), $I_{Nav1.6}$ (downward deflections, third row), and I_{Kv} (upward deflections, fourth row) at ge:gi = 1.5 or 2 are shown. **(A)** Firing activity with $I_{Nav1.6}$ set to zero (control). See also main manuscript Fig. 5 for comparison. **(B, C)** Introducing virtual $I_{Nav1.6}$ reduced to 10 or 20 % of control into the model cell while keeping $I_{Nav1.2}$ unchanged, results in a considerably increased activity. **(D, E)** Typical firing in response with $I_{Nav1.2}$ set to zero and $g_{Nav1.6}$ set to 0.5 or 1. The latter value results in depolarization block at ge:gi = 2 (red arrows). Shaded insets in D show typical $I_{Nav1.6}$ and I_{Kv} traces on expanded time scale.

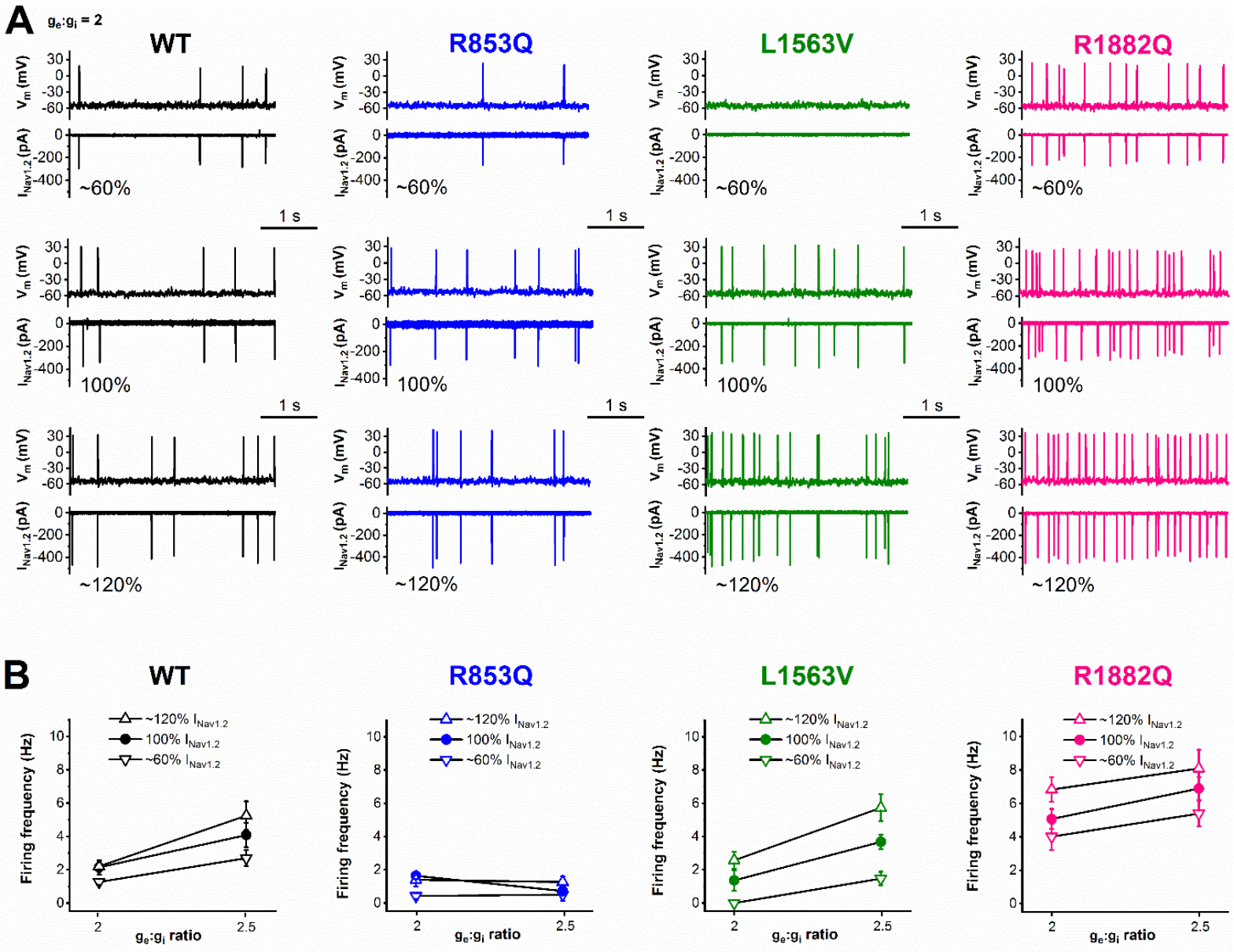

Supplemental Figure S7. The effect of scaling the wild-type or mutant input $I_{Nav1.2}$ on AIS compartment model activity. **(A)** Representative activities in response to a synaptic stimulation of $g_e:g_i = 2$. The input $I_{Nav1.2}$ was reduced (60 %) or increased (120 %) compared to control (100%). V_m changes (upward deflections) and associated scaled input $I_{Nav1.2}$ (downward deflections) are shown. Note the overall firing rate-increase with the R1882Q variant. **(B)** Average firing activity in response to synaptic stimulation of $g_e:g_i = 2$ or 2.5, with scaled input $I_{Nav1.2}$. Data are presented as mean ± SEM; for each data point $n \geq 4$.

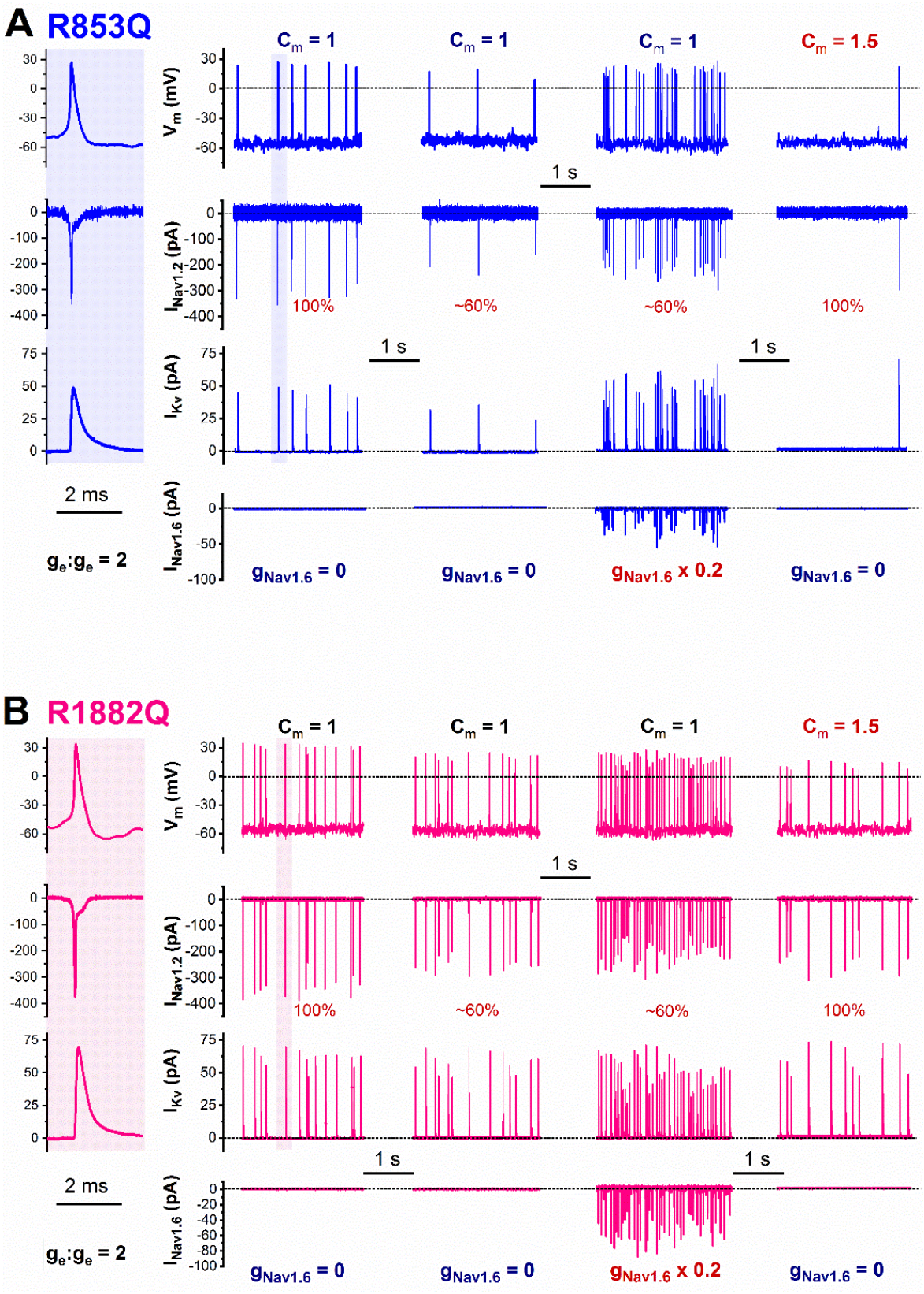

Supplemental Figure S8. Representative action potentials and associated currents in dynamic action potential clamp experiments implementing wild-type **(A)** or R1882Q $I_{Nav1.2}$ **(B)**. The effect of reducing the input $I_{Nav1.2}$ (60 % of control), reducing $I_{Nav1.2}$ (60 % of control) and introducing $I_{Nav1.6}$ (20 % of control), or increasing Cm (by 50 % compared to control). Shaded boxes (left) show typical action potentials and associated $I_{Nav1.2}$ and I_{Kv} traces on expanded time scale. Note the overall higher activity recorded in the AIS model in the presence of R1882Q $I_{Nav1.2}$ compared to R853Q ($n \geq 3$ for both A and B).

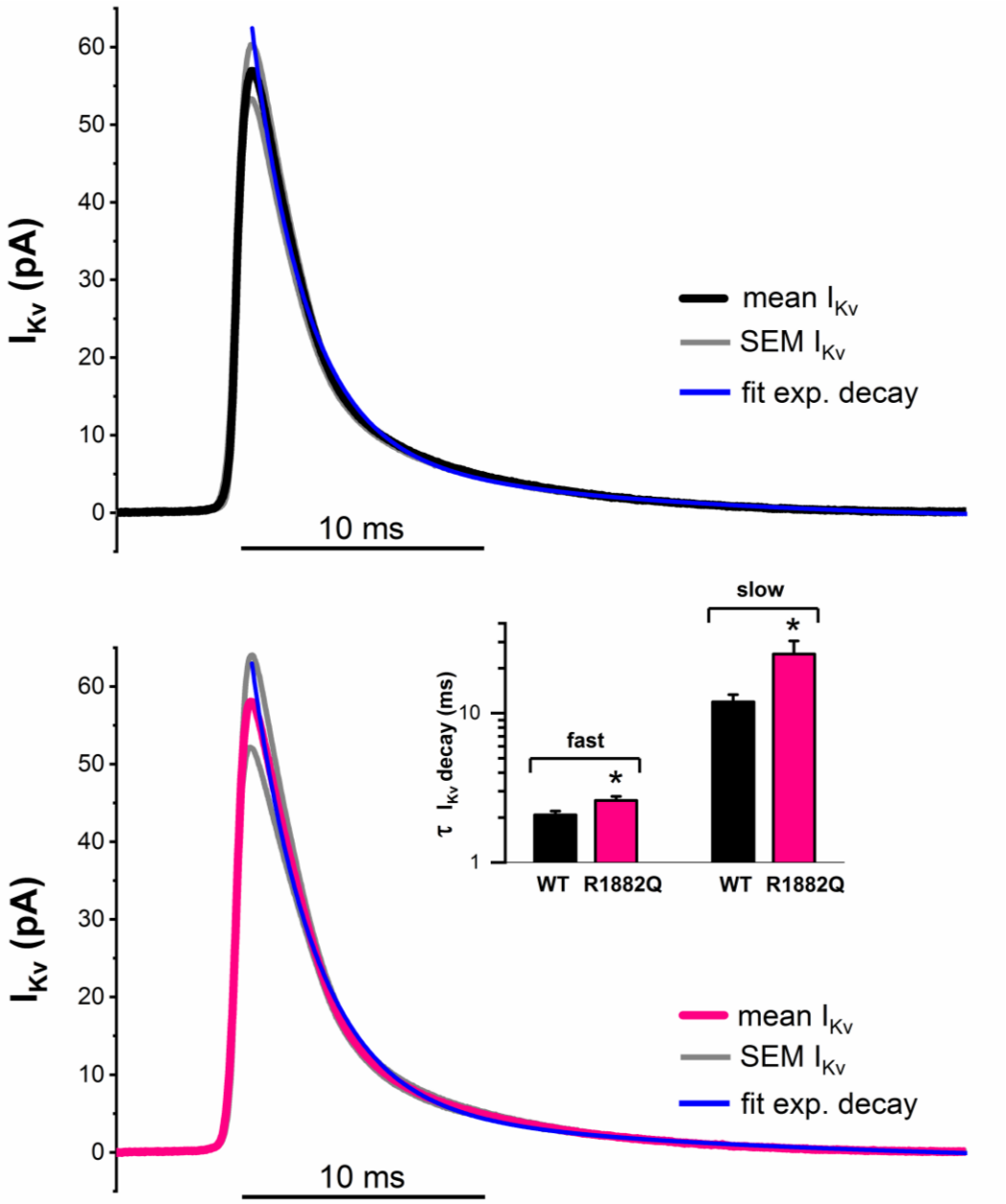

Supplemental Figure S9. The magnitude of I_{Kv} and the time course of I_{Kv} decay in dynamic clamp experiments implementing wild-type (n = 5, top) or R1882Q $I_{Nav1.2}$ (n = 4, bottom). Mean I_{Kv} was determined by averaging the first eight to twelve action potential-associated I_{Kv} traces using data shown in Fig. S7 (at g_e:g_i = 2). For both 'wild-type' and 'R1882Q', the peak I_{Kv} values were similar, 56.9 ± 3.5 pA and 58.1± 5.9 pA, respectively. The time course of mean I_{Kv} decay was fitted with a double-exponential equation (blue traces, top and bottom panels):

$$\frac{I}{I_{max}} = A_f e^{-t/\tau_f} + A_s e^{-t/\tau_s},$$

where t is time, A_f and A_s are the fractions of the fast and slow inactivation components, whereas τ_f and τ_s are the time constants of the fast and slow inactivating components, respectively. Note that I_{Kv} traces in grey represent SEM. With wild-type or R1882Q input $I_{Nav1.2}$, the mean ± SEM values of τ_f were 2.1 ± 0.1 or 2.6 ± 0.2 ms, whereas the mean ± SEM τ_s values were 11.9 ± 1.4 or 24.9 ± 5.59 ms, respectively (inset bar graph; *P<0.05, Student's *t*-test).

APPENDIX

Simulink model of a single compartment axon initial segment (AIS)

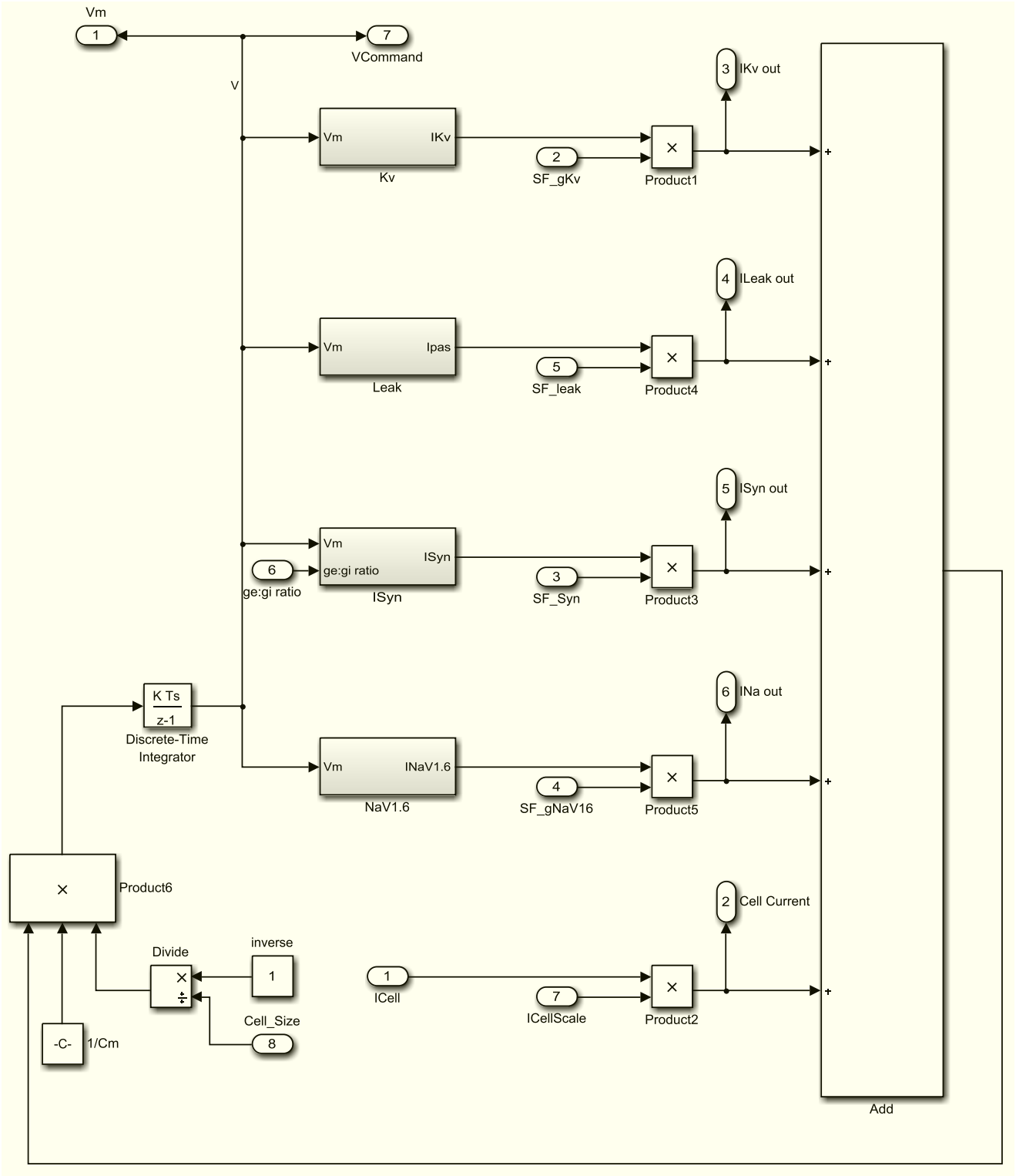

Figure A1. Simulink model of the AIS compartment implementing scalable cell capacitance (Cm) and scalable (SF)currents, including voltage dependent potassium current (I_{Kv}), passive leak current (I_{pas}), voltage dependent $Na_v1.6$ current ($I_{Nav1.6}$), excitatory and inhibitory synaptic currents (I_{Syn}), and heterologously expressed input $Na_v1.2$ current (I_{Cell}).

The characteristics of passive and active components of our AIS compartment model are identical to the published model and are described in detail in the online version of paper by Hu et al (17). The Hu model is based on a previously published multi-compartment model underlying the full dendritic and somatic structure of a layer 5 cortical pyramidal cell (18), containing sodium current data (19, 20) and potassium current data (20, 21) obtained at room temperature (23°C). Our compartment model has uniformly distributed ion channels and it is run at 23°C to match $I_{Nav1.2}$ recording conditions. Similarly, our synaptic noise model is also based on published data (22).

At each iteration of the model, the Vm is calculated by solving the equation:

$$(C * CellSize)\frac{dVm}{dt} = SF\_gKv * I_{Kv} + SF\_leak * I_{pas} + SF\_Syn * I_{Syn}$$

$$+SF\_gNaV1.6 * I_{NaV1.6} + ICellScale * I_{Cell}$$

where C is the capacitance of the compartment, CellSize is a scaling factor to change cell size and Vm is the membrane potential. $SF_{gKv,}$ $SF_{leak,}$ SF_{Syn} , $SFg_{Nav,}$ and $I_{CellScale}$ are scaling factors for I_{Kv}, I_{pas}, I_{Syn}, and $I_{Nav1.6}$, respectively, whereas $I_{CellScale}$ is the scaling factor for I_{Cell} (the external input $Na_v1.2$ current). In all experiments, the voltage dependent $Na_{v1.6}$ current was set to zero unless stated otherwise.

The panels below show the nested models of the individual current components described using the Hodgkin-Huxley formalism (23).

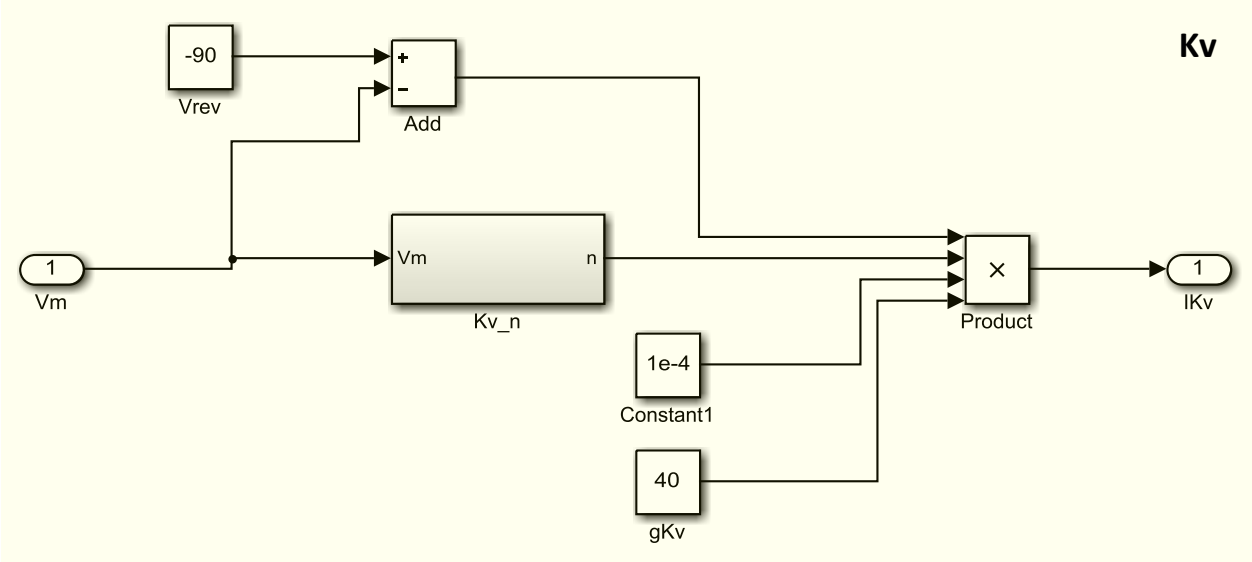

Figure A1.1. Potassium current (Kv)

$$I_{Kv} = gKv * n(Vm - (-90)),$$

where $gKv = 40\ pS\mu m^{-2}$ is the potassium conductance and n is the activation gate.

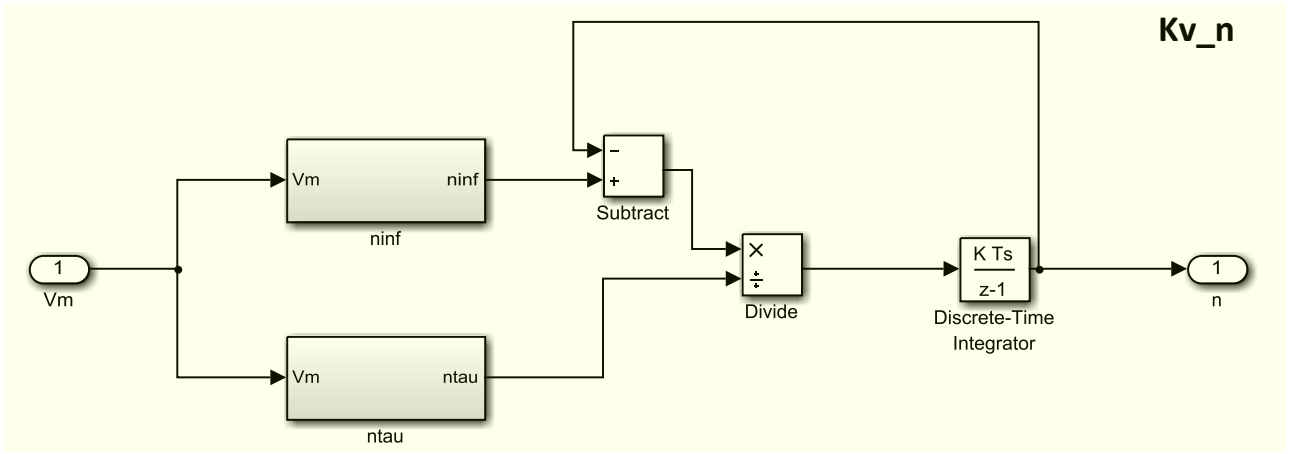

Figure A1.1.1. Potassium channel activation gate (Kv_n)

$$\frac{dn}{dt} = \frac{n_{inf} - n}{n_{tau}}$$

where n_{inf}, n_{tau} are the steady-state activation variable and time constant of activation, respectively.

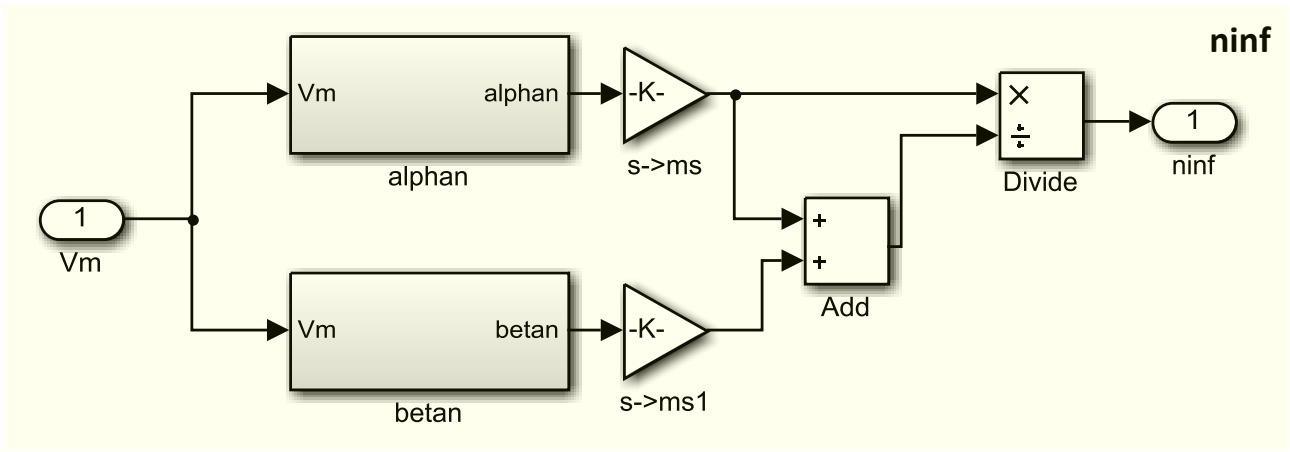

Figure A1.1.1.1. Steady state activation of potassium ion channel (ninf).

$$ninf = \frac{alphan}{alphan + betan}$$

where $alphan$ and $betan$ are rate constants of potassium activation.

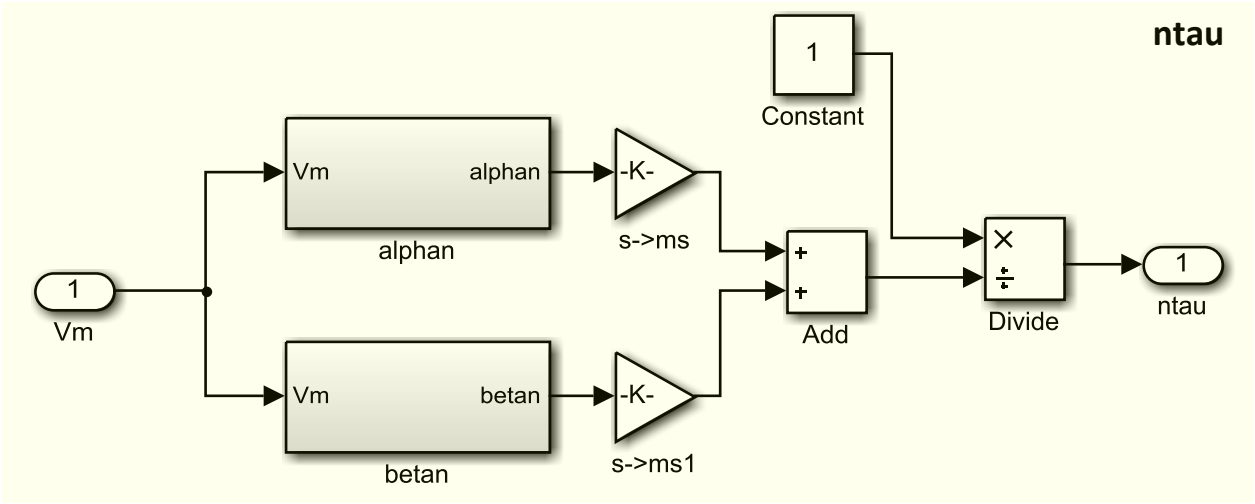

Figure A1.1.1.2. Activation time constant of potassium ion channel (ntau).

$$ntau = \frac{1}{alphan + betan}$$

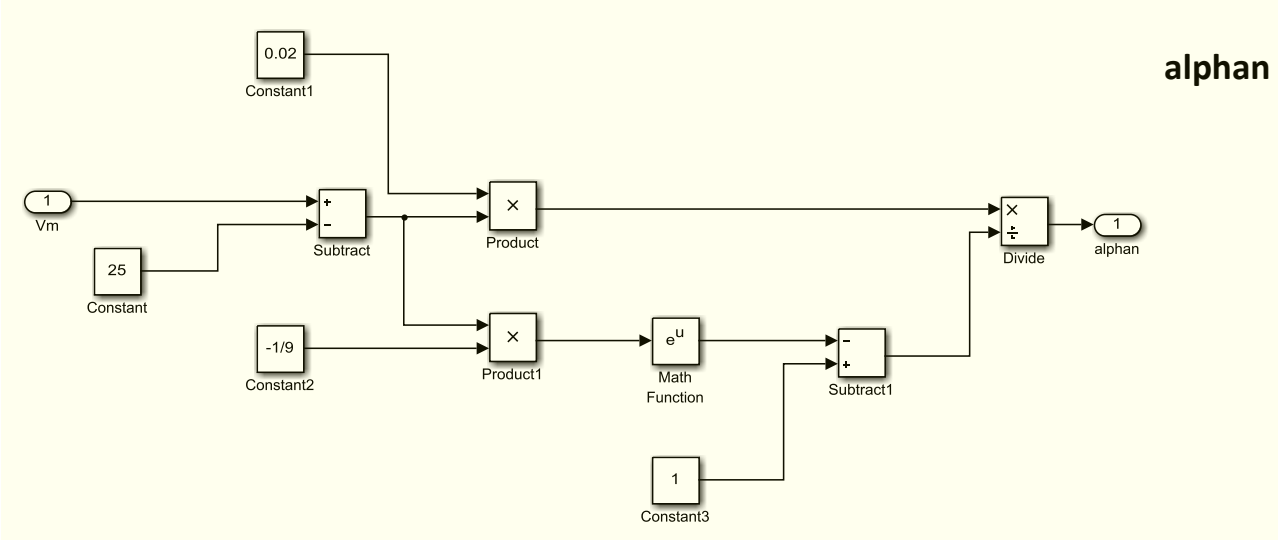

Figure A1.1.1.2.1. Rate constant (alphan).

$$alphan = \frac{0.02(Vm - 25)}{1 - \exp\left(-\frac{Vm - 25}{9}\right)}$$

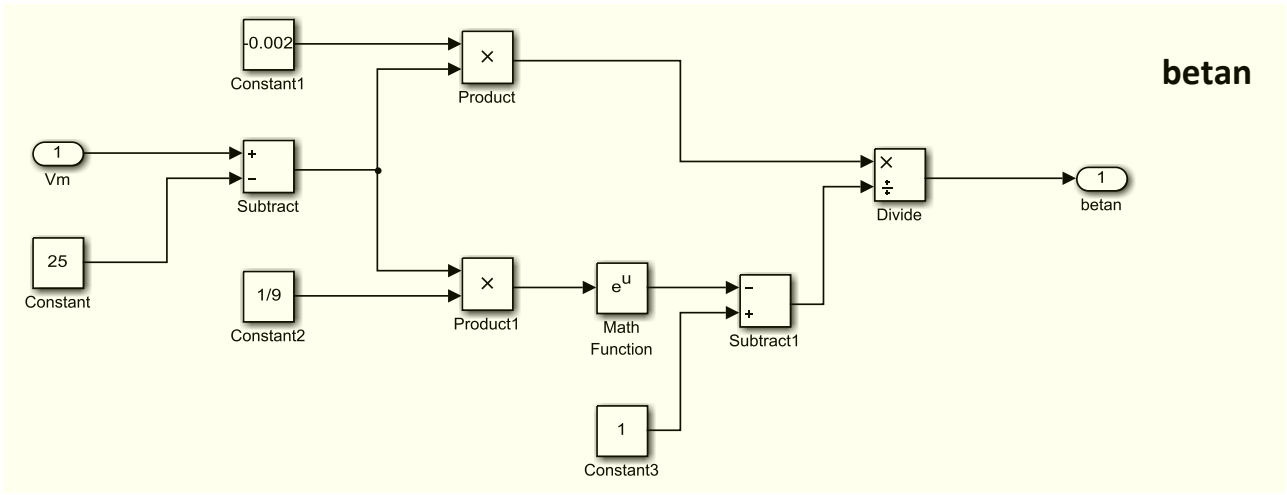

Figure A1.1.1.2.2. Rate constant (betan).

$$betan = \frac{-0.002(Vm - 25)}{1 - \exp\left(\frac{Vm - 25}{9}\right)}$$

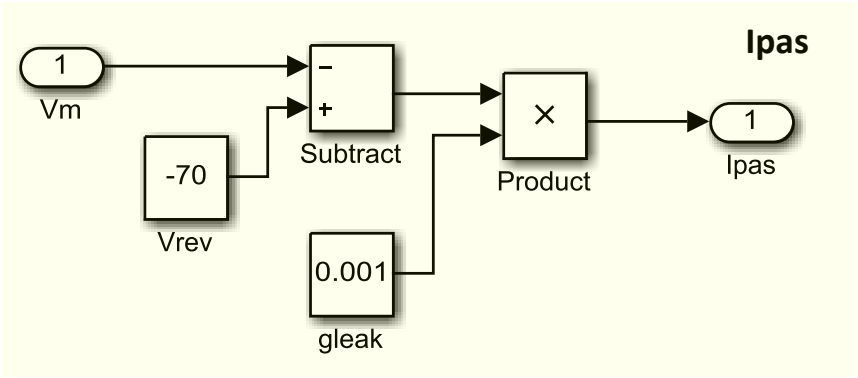

Figure A1.2. Leak current (Ipas).

$$Ipas = 0.001 * (Vm - (-70))$$

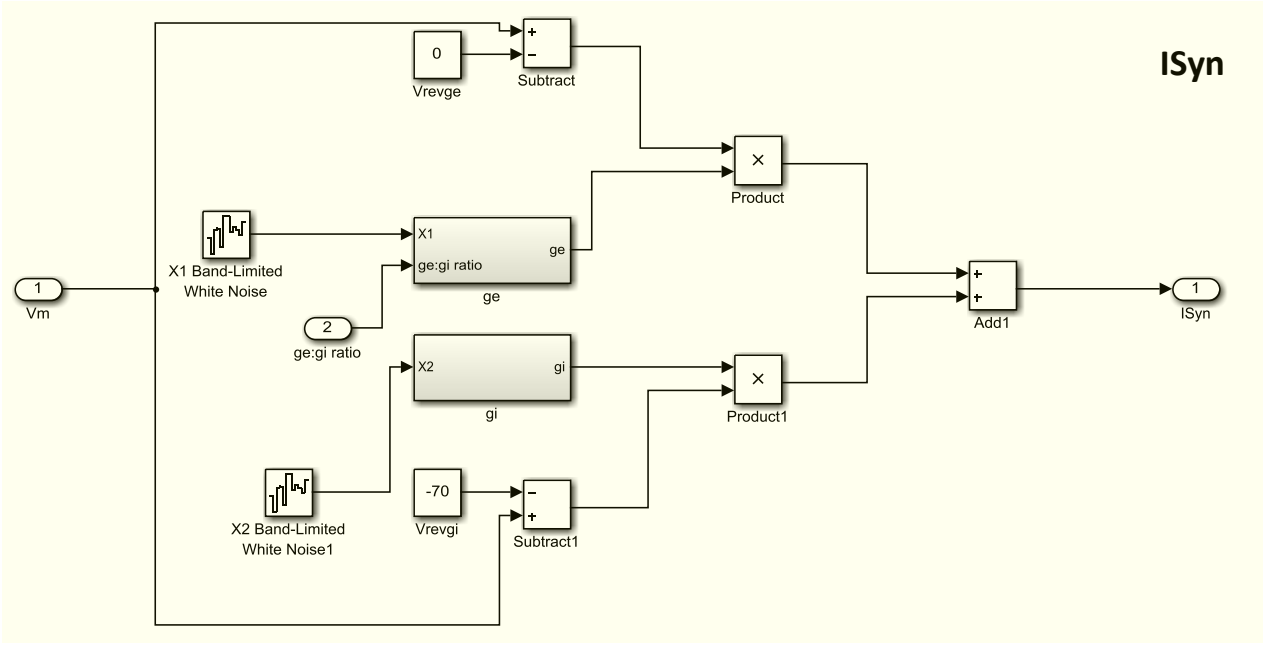

Figure A1.3. Synaptic current (ISyn).

$$ISyn = ge(Vm - 0) + gi\big(Vm - (-70)\big),$$

where ge, gi are excitatory and inhibitory synaptic conductances, respectively.

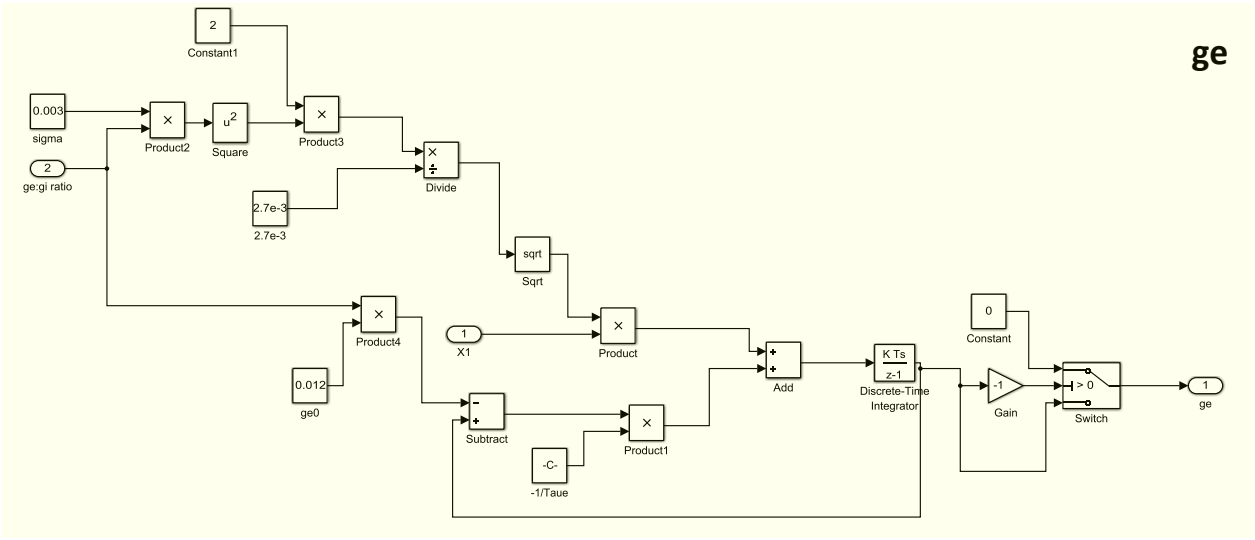

Figure A1.3.1. Excitatory conductance (ge).

$$\frac{dge}{dt} = -\frac{1}{taue}[ge - ge_0] + \sqrt{D_e}x1$$

$$D_e = 2 * \frac{sigmae^2}{taue}$$

where $taue = 2.7\,ms, ge0 = 0.012\,\mu S,\ sigmae = 0.003\,\mu S, D_e$ is the time constant, average standard deviation, and amplitude of the excitatory conductance, respectively, and x_1 is Gaussian white noise of zero mean and unit standard deviation.

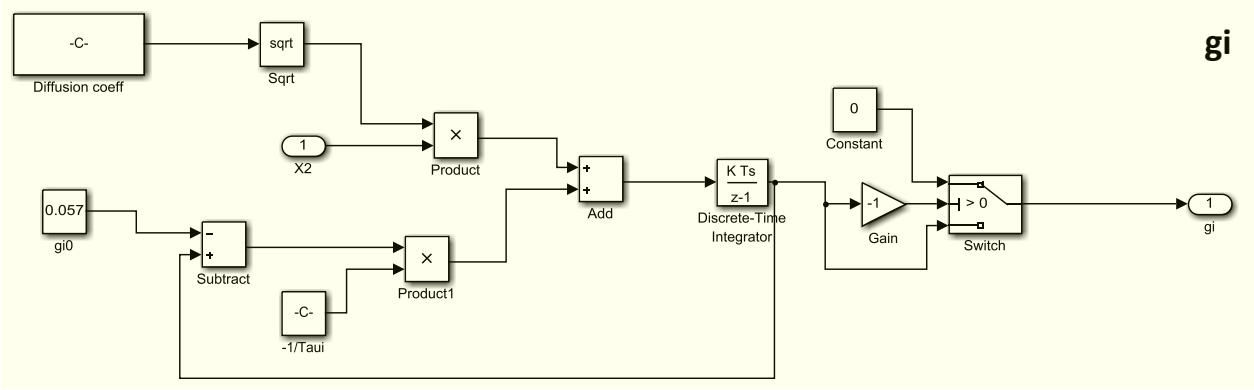

Figure A1.3.2. Inhibitory conductance (gi).

$$\frac{dgi}{dt} = -\frac{1}{taui}[gi - gi_0] + \sqrt{D_i}x_2$$

$$D_i = 2 * \frac{sigmai^2}{taui}$$

where $taui = 10.5\, ms, gi0 = 0.057\, \mu S,\ sigmai = 0.0066\, \mu S, D_i$ is the time constant, average standard deviation, and amplitude of the inhibitory conductance, respectively, and x_2 is Gaussian white noise of zero mean and unit standard deviation.

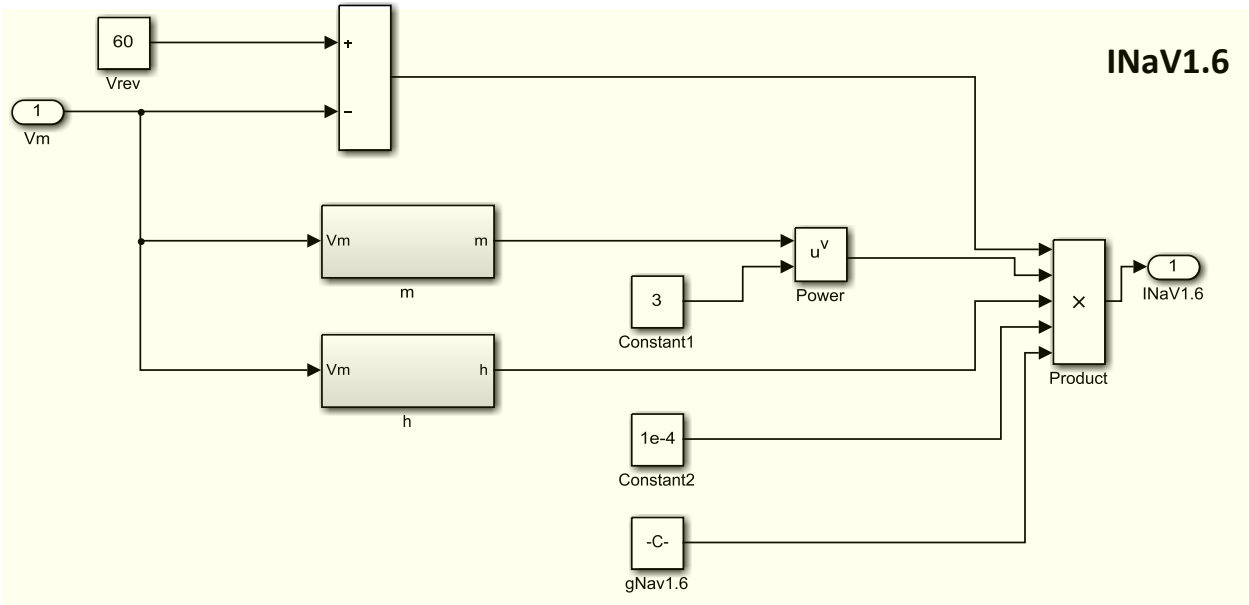

Figure A1.4. Sodium ($Na_v1.6$) current (INaV1.6).vv

$$INaV1.6 = gNav1.6 * m^3h(Vm - (-60))$$

where $gNav1.6 = 1097.1\ pS\mu m^{-2}$ is the sodium conductance, m, h are activation and inactivation gates, respectively.

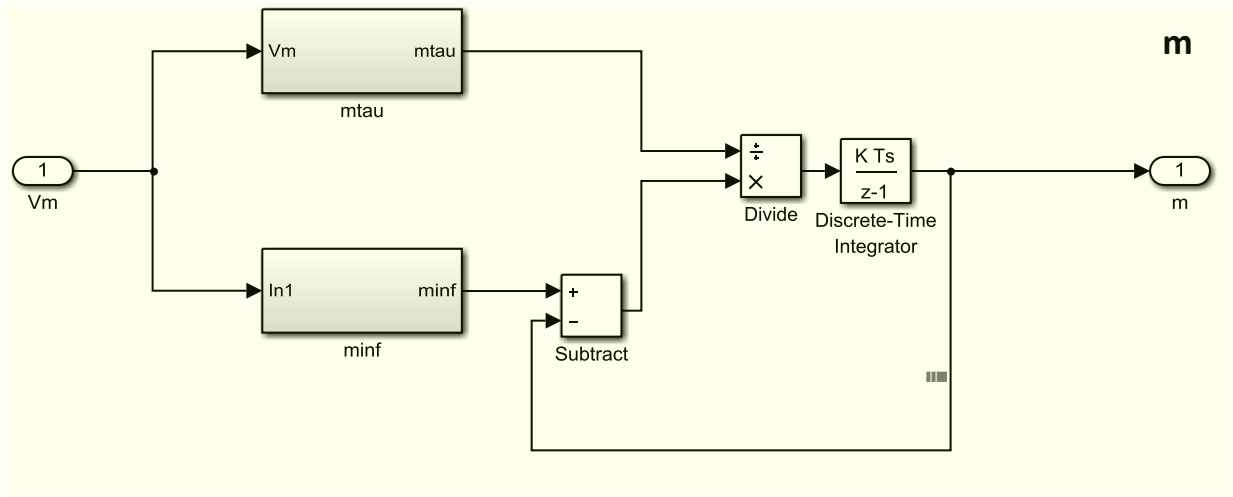

Figure A1.4.1. Sodium activation gate (m).

$$\frac{dm}{dt} = \frac{m_{inf} - m}{m_{tau}}$$

where m_{inf}, m_{tau} are the steady state activation and activation time constants, respectively.

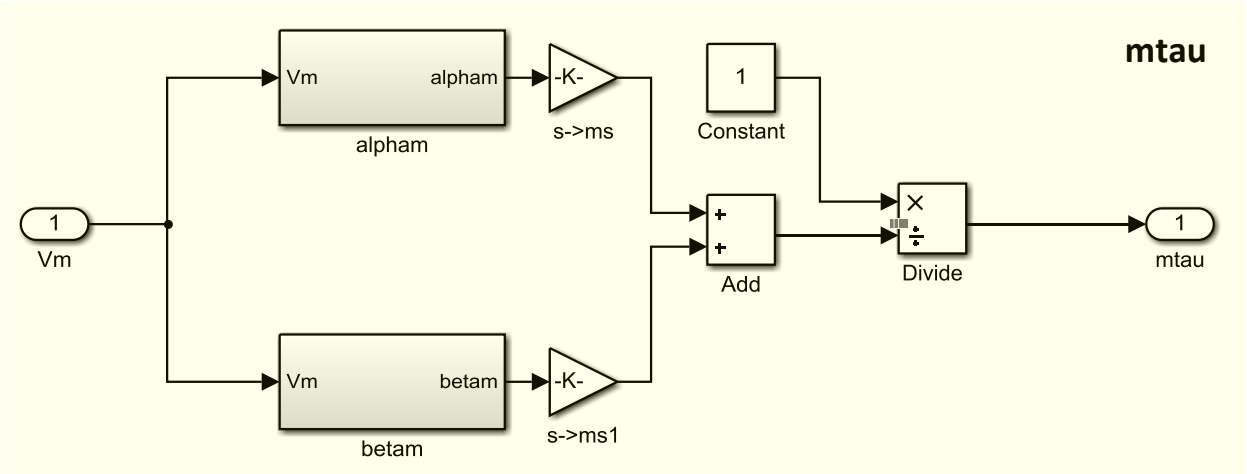

Figure A1.4.1.1. Activation time constant of sodium ion channel (mtau).

$$mtau = \frac{1}{alpham + betam}$$

where $alpham$ and $betam$ are rate constants, respectively.

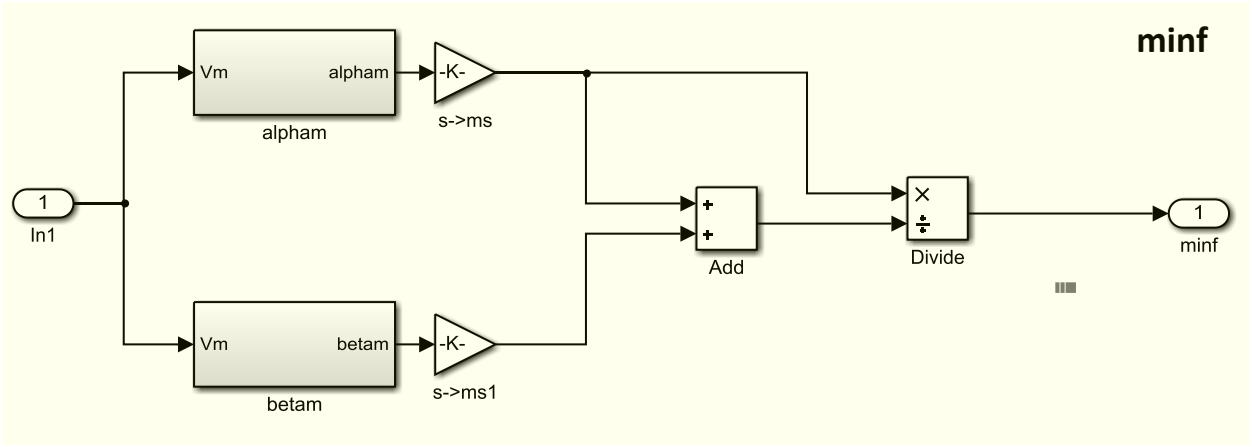

Figure A1.4.1.2. Steady-state activation of sodium ion channel (minf).

$$minf = \frac{alpham}{alpham + betam}$$

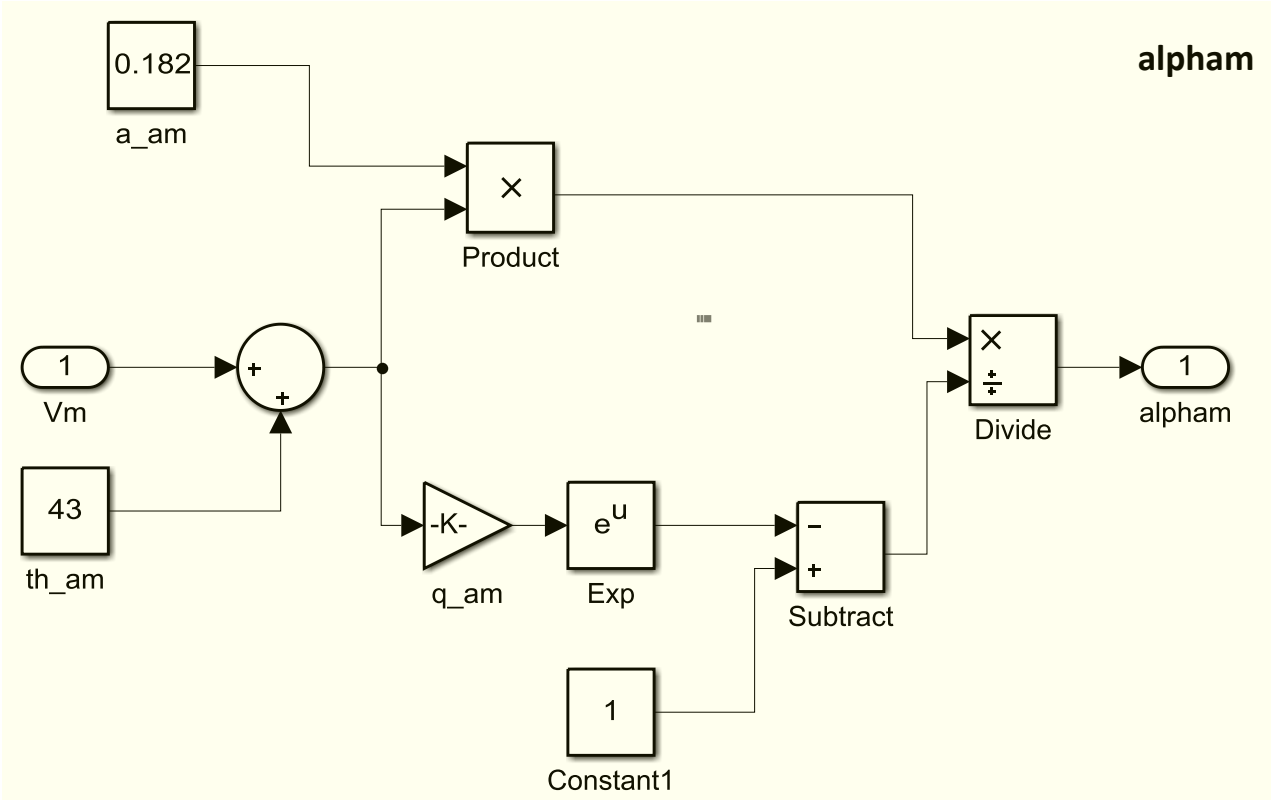

Figure A1.4.1.2.1. Rate constant (alpham).

$$alpham = \frac{0.182(Vm + 43)}{1 - \exp(-\frac{Vm + 43}{6})}$$

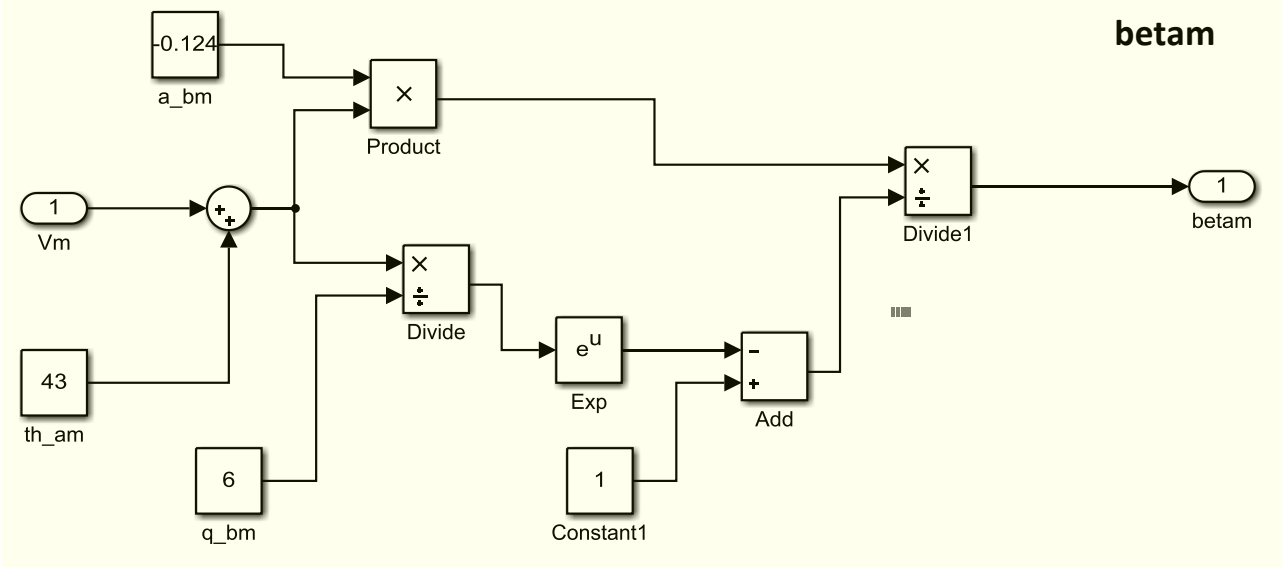

Figure A1.4.1.2.2. Rate constant (betam).

$$betam = \frac{-0.124(Vm + 43)}{1 - \exp(\frac{Vm + 43}{6})}$$

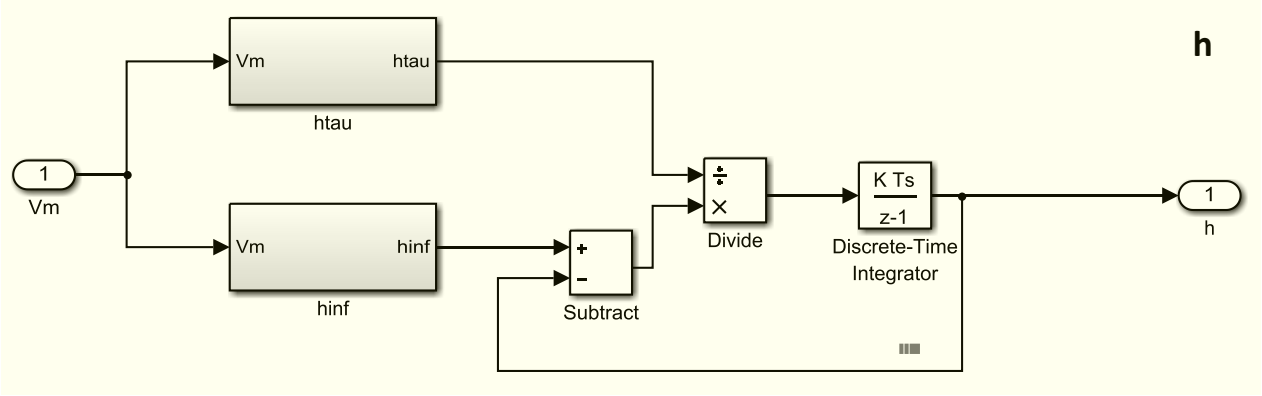

Figure A1.4.2. Sodium channel inactivation gate (h).

$$\frac{dh}{dt} = \frac{h_{inf} - h}{h_{tau}}$$

where h_{inf}, h_{tau} are the steady state inactivation and inactivation time constants, respectively.

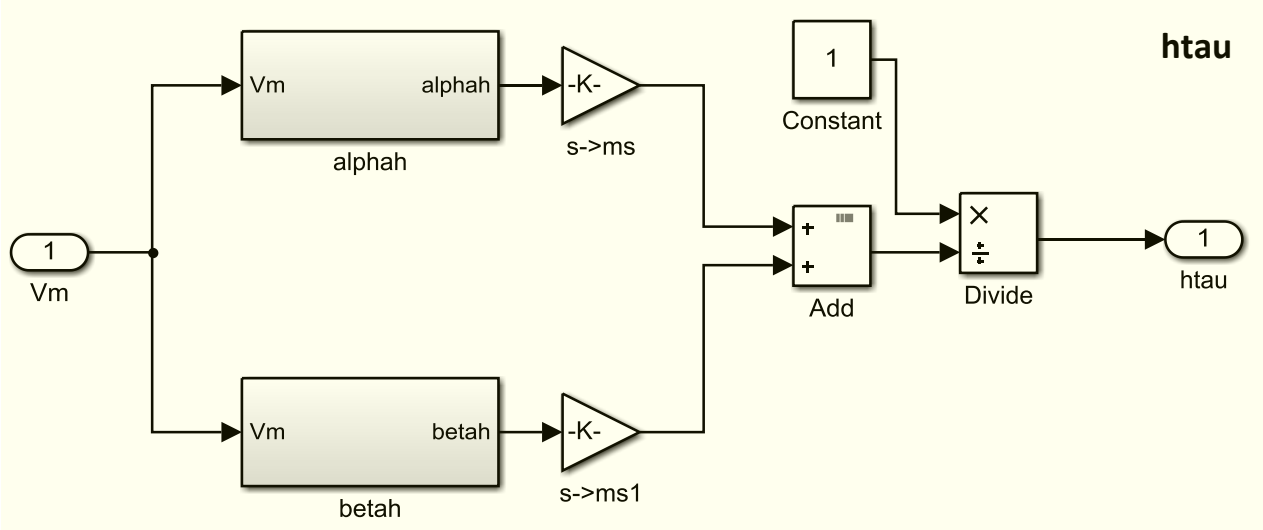

Figure A1.4.2.1. Sodium channel inactivation time constant (htau).

$$htau = \frac{1}{alphah + betah}$$

where $alphah$ and $betah$ are rate constants of inactivation, respectively.

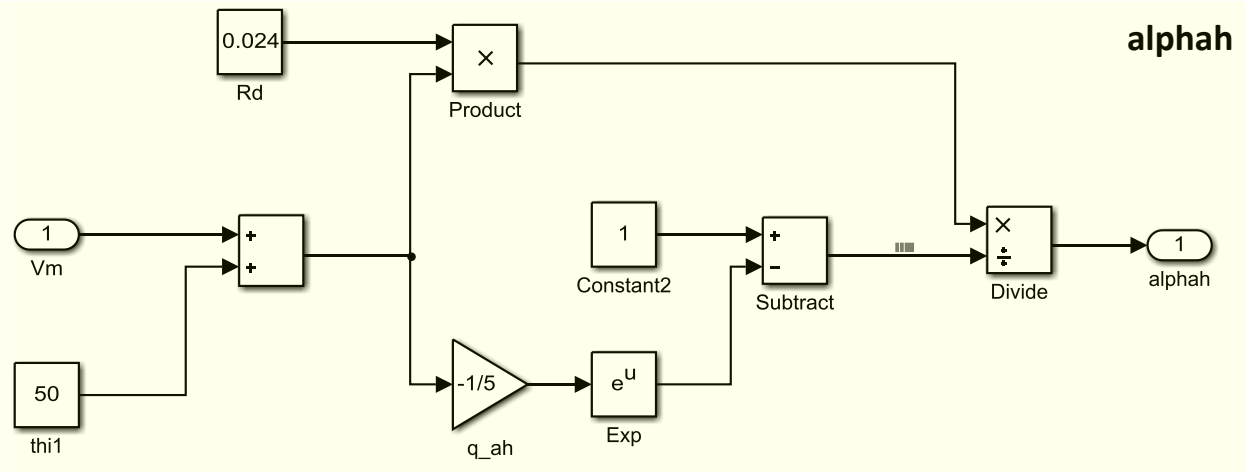

Figure A1.4.2.1.1. Rate constant (alphah).

$$alphah = \frac{0.024(Vm + 50)}{1 - \exp(-\frac{Vm + 50}{5})}$$

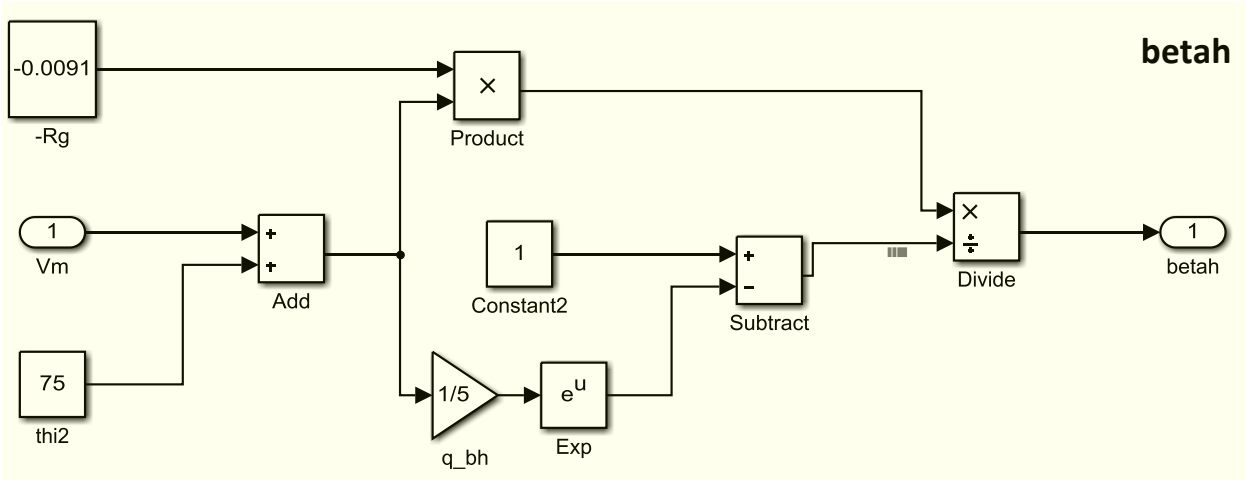

Figure A1.4.2.1.2. Rate constant (betah).

$$betah = \frac{-0.0091(Vm + 75)}{1 - \exp(\frac{Vm + 75}{5})}$$

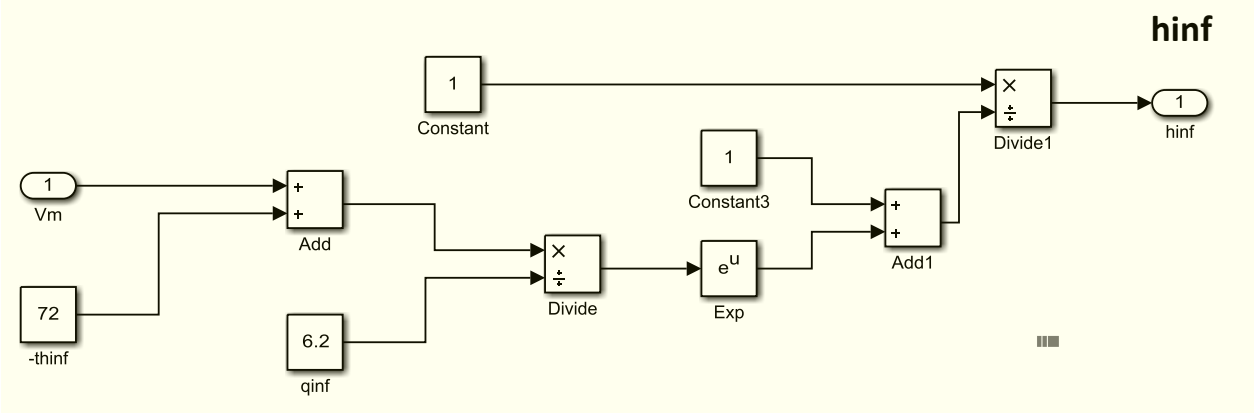

Figure A1.4.2.2. Sodium channel steady-state inactivation (hinf).

$$hinf = \frac{1}{1 + \exp(\frac{Vm + 72}{6.2})}$$

References

1. Howell KB*, et al.* (2015) SCN2A encephalopathy: A major cause of epilepsy of infancy with migrating focal seizures. *Neurology* 85(11):958-966.
2. Nakamura K*, et al.* (2013) Clinical spectrum of *SCN2A* mutations expanding to Ohtahara syndrome. *Neurology* 81(11):992-998.
3. Epi KC*, et al.* (2013) *De novo* mutations in epileptic encephalopathies. *Nature* 501(7466):217-221.
4. Carvill GL*, et al.* (2013) Targeted resequencing in epileptic encephalopathies identifies de novo mutations in *CHD2* and *SYNGAP1*. *Nature genetics* 45(7):825-830.
5. Samanta D & Ramakrishnaiah R (2015) *De novo* R853Q mutation of *SCN2A* gene and West syndrome. *Acta neurologica Belgica* 115(4):773-776.
6. Wolff M*, et al.* (2017) Genetic and phenotypic heterogeneity suggest therapeutic implications in *SCN2A*-related disorders. *Brain* 140(5):1316-1336.
7. Trump N*, et al.* (2016) Improving diagnosis and broadening the phenotypes in early-onset seizure and severe developmental delay disorders through gene panel analysis. *Journal of medical genetics* 53(5):310-317.
8. Kobayashi Y*, et al.* (2016) High prevalence of genetic alterations in early-onset epileptic encephalopathies associated with infantile movement disorders. *Brain Dev* 38(3):285-292.
9. Li J*, et al.* (2016) Genes with *de novo* mutations are shared by four neuropsychiatric disorders discovered from NPdenovo database. *Molecular psychiatry* 21(2):290-297.
10. Xu R*, et al.* (2007) A childhood epilepsy mutation reveals a role for developmentally regulated splicing of a sodium channel. *Mol Cell Neurosci* 35(2):292-301.
11. West JW, Scheuer T, Maechler L, & Catterall WA (1992) Efficient expression of rat brain type IIA Na^+ channel α subunits in a somatic cell line. *Neuron* 8(1):59-70.
12. Cohen CJ, Bean BP, & Tsien RW (1984) Maximal upstroke velocity as an index of available sodium conductance. Comparison of maximal upstroke velocity and voltage clamp measurements of sodium current in rabbit Purkinje fibers. *Circ Res* 54(6):636-651.
13. Chadda KR, Jeevaratnam K, Lei M, & Huang CL (2017) Sodium channel biophysics, late sodium current and genetic arrhythmic syndromes. *Pflugers Arch* 469(5-6):629-641.
14. Jung HY, Mickus T, & Spruston N (1997) Prolonged sodium channel inactivation contributes to dendritic action potential attenuation in hippocampal pyramidal neurons. *J Neurosci* 17(17):6639-6646.
15. Vilin YY, Makita N, George AL, Jr., & Ruben PC (1999) Structural determinants of slow inactivation in human cardiac and skeletal muscle sodium channels. *Biophys J* 77(3):1384-1393.
16. Sokolov S, Scheuer T, & Catterall WA (2010) Ion permeation and block of the gating pore in the voltage sensor of $Na_v1.4$ channels with hypokalemic periodic paralysis mutations. *J Gen Physiol* 136(2):225-236.
17. Hu W*, et al.* (2009) Distinct contributions of $Na_v1.6$ and $Na_v1.2$ in action potential initiation and backpropagation. *Nat Neurosci* 12(8):996-1002.
18. Mainen ZF & Sejnowski TJ (1996) Influence of dendritic structure on firing pattern in model neocortical neurons. *Nature* 382(6589):363-366.
19. Huguenard JR, Hamill OP, & Prince DA (1988) Developmental changes in Na^+ conductances in rat neocortical neurons: appearance of a slowly inactivating component. *Journal of neurophysiology* 59(3):778-795.
20. Hamill OP, Huguenard JR, & Prince DA (1991) Patch-clamp studies of voltage-gated currents in identified neurons of the rat cerebral cortex. *Cerebral cortex* 1(1):48-61.

21. Sah P & McLachlan EM (1992) Potassium currents contributing to action potential repolarization and the afterhyperpolarization in rat vagal motoneurons. *Journal of neurophysiology* 68(5):1834-1841.
22. Destexhe A, Rudolph M, Fellous JM, & Sejnowski TJ (2001) Fluctuating synaptic conductances recreate *in vivo*-like activity in neocortical neurons. *Neuroscience* 107(1):13-24.
23. Hodgkin AL & Huxley AF (1952) A quantitative description of membrane current and its application to conduction and excitation in nerve. *J Physiol* 117(4):500-544.